

# Dynamics of PAR proteins explain the oscillation and ratcheting mechanisms in dorsal closure

C.H. Durney<sup>1</sup>, T.J.C. Harris<sup>2</sup>, J.J. Feng<sup>1,3\*</sup>

<sup>1</sup> Department of Mathematics, University of British Columbia, Vancouver, British Columbia, Canada

<sup>2</sup> Department of Cell & Systems Biology, University of Toronto, Toronto, Ontario, Canada

<sup>3</sup> Department of Chemical and Biological Engineering, University of British Columbia, Vancouver, British Columbia, Canada

## Abstract

We present a vertex-based model for *Drosophila* dorsal closure that predicts the mechanics of cell oscillation and contraction from the dynamics of the PAR proteins. Based on experimental observations of how aPKC, Par-6 and Bazooka translocate from the circumference of the apical surface to the medial domain, and how they interact with each other and ultimately regulate the apicomedial actomyosin, we formulate a system of differential equations that capture the key features of dorsal closure, including distinctive behaviors in its early, slow and fast phases. The oscillation in cell area in the early phase of dorsal closure results from an intracellular negative feedback loop that involves myosin, an actomyosin regulator, aPKC and Bazooka. In the slow phase, gradual sequestration of apicomedial aPKC by Bazooka clusters causes incomplete disassembly of the actomyosin network over each cycle of oscillation, thus producing a so-called ratchet. The fast phase of rapid cell and tissue contraction arises when medial myosin, no longer antagonized by aPKC, builds up in time and produces sustained contraction. Thus, a minimal set of rules governing the dynamics of the PAR proteins, extracted from experimental observations, can account for all major mechanical outcomes of dorsal closure, including the transitions between its three distinct phases.

Insert Received for publication Date and in final form Date.

\*james.feng@ubc.ca

## INTRODUCTION

Dorsal closure (DC) is an important morphogenetic process during the embryonic development of *Drosophila*. During DC, two flanking epidermal tissues are fused together to close an opening on the dorsal side of the embryo, covering up the thin amnioserosa (AS) tissue. The entire DC process, lasting about 3.5 hours, exhibits three distinct phases showing great spatial and temporal coordination. The early phase is characterized by AS cell oscillations and no loss in overall tissue area. The ensuing slow phase exhibits a gradual loss in overall tissue area and a dampening of cellular oscillations. Finally, the fast phase displays rapid and persistent loss of tissue area and cessation of the oscillations. While recent experiments have identified several contributing factors in dorsal closure (1–6), the connections between them remain elusive.

For the early phase, the key question is the cause of the cyclic oscillation of the cell area. On the apical surface, a medial network of actomyosin periodically assembles and disassembles, with a period of approximately 4 minutes (1, 7–9). The cell contracts following the assembly of the actomyosin network, and relaxes when the network disassembles (7, 10). After each

cycle, the cell area returns to more or less the previous state. The contraction of one cell pulls on its neighbors, yielding a preference for antiphase pulsing between neighboring cells (1). But Blanchard et al. (4) have also observed transient “ribbons” of cells that are simultaneously contracting or expanding. It remains to be ascertained whether the oscillatory behavior originates from the autonomous dynamics within each cell or from the communications between neighbors, or even both (1, 11, 12).

Naturally one seeks an explanation for the oscillatory behavior from biochemical signaling (7, 13–16). David et al. (7) highlighted the roles of the PAR proteins. Bazooka (Baz) promotes the duration of actomyosin contraction, while the Par-6/aPKC complex promotes the lull time between contractions. More recently, David et al. (15) further delineated the spatial and temporal relationship among the PAR proteins and the actomyosin network that periodically assembles in the apicomedial domain of the AS cells. The actomyosin recruits aPKC from the circumference of the apical surface toward the medial region, where it forms puncta that colocalize with the actomyosin network. In turn, aPKC recruits Bazooka into the medial region. As aPKC is known to phosphorylate and inhibit myosin (17, 18), and causes apical relaxation in AS cells (7), while Baz promotes apical constriction through complexing aPKC (7), David et al. (15) hypothesized that the PAR proteins form a negative feedback loop with the medial actomyosin network to produce the oscillatory outcome. The expansion phase of the oscillation may be driven by the elasticity of the AS cells and the contraction of neighboring cells.

To rationalize the areal contraction of the slow phase, the two central ideas are the ratcheting mechanism and the supra-cellular actin cable, although recent evidence has also suggested cell volume loss as a contributor (19). The concept of an intracellular or internal ratchet was introduced by Martin et al. (10, 20) to explain the pulsed constriction of *Drosophila* ventral furrow cells. After each contraction, a cell is prevented from returning to its prior apical area by tension emanating from an apicomedial actomyosin meshwork, which stabilizes the cell shape and produce net constriction. Consistent with the above, the live images of David et al. (7, 15) demonstrate an apicomedial actomyosin network that grows stronger over each pulse in the slow phase, a transition that coincides with greater aPKC-Baz interaction in the medial domain. Roughly concurrent with the onset of the slow phase, an actin cable appears along the boundary between the AS tissue and the surrounding epidermis. It encircles the AS like a purse string and clamps down on the tissue. This was initially considered the main cause of AS contraction (1, 21), but more recent work has challenged its importance (9, 20, 22–24). For example, Wells et al. (9) disrupted the purse string by severing one or both of the canthi and observed that closure proceeded normally. Pasakarnis et al. (23) used selective force elimination to demonstrate that the amnioserosa cells alone are capable of driving dorsal closure. Ducuing and Vincent (24) reported that the actin cable does not contribute appreciably to the dorsal-ward movement of the leading edges. Thus, a consensus seems to be forming on a secondary role for the actin cable.

The advent of the fast phase brings a few new factors. As the AS tissue narrows, the opposing epidermis extends filopodia onto the opposite side, which then pull to help the closure (25–27). This is known as zippering. Much like the actin cable, the zippering forces have been shown to be superfluous for complete closure (9). Moreover, AS cell apoptosis contributes to rapid closure by dropping out of the plane of the amnioserosa, effectively reducing the tissue area (3, 8, 21, 28). Finally, the epidermis may elongate actively to assist rapid closure in the fast phase (29).

Mathematical modeling has been used to integrate the experimental insights above into a more precise and quantitative understanding (26, 30, 31). A majority of these models are purely mechanical, imposing prescribed forces on the tissue (32) or on individual cells (1, 33) and examining their elastic or viscoelastic responses (34, 35). In such models, the cellular oscillations of the early phase is the result of an externally imposed force or the mechanical coupling between cells (1, 32). More recent work strove to integrate the mechanical and biochemical aspects of the process (36, 37). Wang et al. (22) assumed a simple kinetic equation for a hypothetical signaling molecule, and predicted cyclic myosin dynamics for the early phase from a negative feedback loop. By an *ad hoc* device of shrinking the resting length of the elastic cell borders, their model produced net loss of cell and tissue area. Similarly, Machado et al. (11) relied on a feedback loop between a putative signaling molecule and actin turnover, which was a proxy for myosin attachment and detachment. This model showed how the rate of actin turnover may modulate the period of AS cell oscillation. These models are commendable in seeking a deeper explanation of the DC dynamics from the chemical-mechanical coupling, but they have incorporated much phenomenology and left several fundamental questions unanswered. What is the mechanism for the spontaneous oscillation in the early phase? What mechanism organizes the ratcheting behavior in the early phase? What triggers the transition from one phase to the next?

These questions have motivated the current model, which integrates earlier vertex models (1, 22) with the biochemical insights of recent experiments (7, 15) to provide a comprehensive picture of dorsal closure. In particular, we will demonstrate how the PAR proteins interact with a regulator of the actomyosin network to produce not only the oscillation in the early phase, but also the ratcheting in the slow phase and the persistent contraction in the fast phase. Essentially all features of the DC process, except for apoptosis of AS cells and zippering that affect the final closure, can be explained by a cell-mechanical framework supplied with a few experimental observations regarding the movement and biochemistry of the PAR proteins.

## MODEL FORMULATION

We represent the amnioserosa tissue by a 2D vertex model of 121 hexagonal cells (Fig. 1a). Since the AS cells are thin and squamous, and the actomyosin and signaling proteins of interest are localized to the apical surface, we adopt a 2D planar representation (22). Each cell has six peripheral nodes connected by passively elastic edges due to the actin cortex. A central node is connected to the circumference by elastic spokes that also have an active force component due to myosin contraction (Fig. 1a inset). The amnioserosa is flanked by an epidermis that resists dorsal closure (21, 38) but can also engage in active elongation (29). As a simplified treatment, we surround the amnioserosa by elastic tension lines (blue lines in Fig. 1a) attached to an outer boundary that is fixed in space.

The mechanical model essentially follows the previous work of Wang et al. (22), and more details can be found in Sec. S1 of the online Supporting Material (SM). In brief, each cell edge or spoke carries a linearly elastic force depending on the elongation or compression of that segment relative to its rest length. Each spoke also carries an active myosin force proportional to the number of myosin motors on it (Eq. S3 in SM), which is in turn determined by the actomyosin regulator to be discussed in the kinetic model below (Eq. S1). Each central or peripheral node executes over-damped motion according to the vector

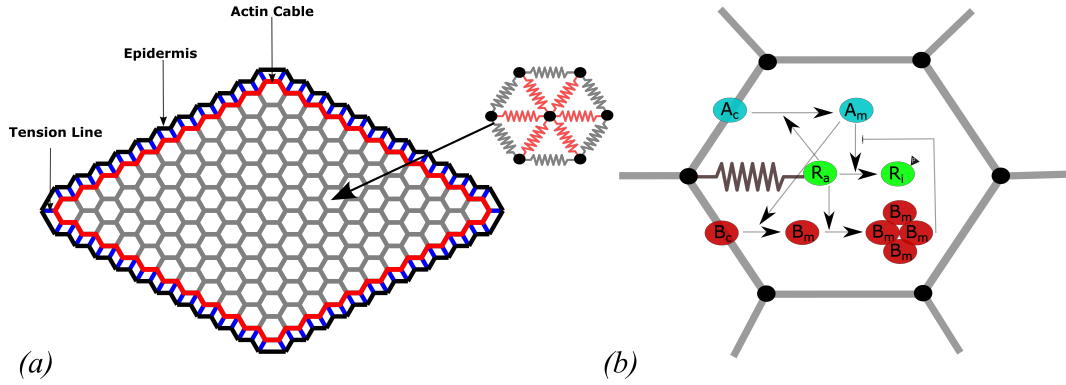


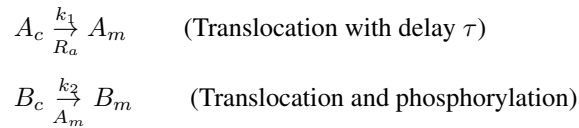
Figure 1: (a) The AS tissue comprises 121 hexagonal cells and the big arrow points to a “representative cell” whose dynamics is reported later in the paper. Each cell has 6 edges (grey) and 6 spokes (red). The edges and spokes are passively elastic represented by springs and the spokes also carry an active myosin force. The AS tissue is linked by blue elastic tension lines to a stationary epidermis (black outline), and the magenta border represents the supracellular actin cable. (b) The translocation and interactions of the PAR proteins inside each cell. Apico-medial actomyosin, represented by its regulator  $R_a$ , recruits apico-circumferential aPKC ( $A_c \rightarrow A_m$ ) medially to form a pool of apico-medial aPKC, which phosphorylates the active regulator  $R_a$  into an inactive form  $R_i$ . Concomitantly,  $A_m$  recruits its own inhibitor Baz medially ( $B_c \rightarrow B_m$ ), which in a clustered form sequesters  $A_m$ .  $R_a$  promotes the clustering of  $B_m$ .

sum of all the edge and spoke forces acting on it (Eq. S4). The supracellular actin cable surrounding the AS tissue is modeled by a contractile force that varies piecewise linearly in time (Eq. S5); the time of onset and duration of linear increase before leveling off are fitted to experimental data. The tension lines connecting the AS to the surroundings are linearly elastic, with a force that balances the AS tissue tension in an average sense. Finally, we neglect zippering forces in our model.

Our kinetic model is novel in its detailed treatment of the molecular signaling pathways, based on observations of the transport and interaction of the PAR proteins (7, 15, 39), the identity of the target protein for aPKC (17, 40–42), and the clustering dynamics of apico-medial Baz (43–45). Figure 1(b) depicts the protein species tracked in our model as well as their spatial localization and interactions. The PAR proteins, Baz, Par-6 and aPKC, have been known to regulate the apico-medial localization and activation of actomyosin in amnioserosa (7, 15). Of the three, PAR-6 always acts in conjunction with aPKC (7, 46), and we will consider the aPKC-Par-6 complex a single entity in the following, referring to it simply as aPKC. Although aPKC is long known to inhibit actomyosin, its target, which is presumably a regulator or effector of RhoA/Rho1, has not been unequivocally identified. In mammalian cells, Smurf1 can be phosphorylated by aPKC to cause RhoA degradation (17), and aPKC may also act through p190RhoGAP to inhibit RhoA (40). More recent evidence points to Rho kinase (Rok) as a likely target, as phosphorylation by aPKC causes Rok to dissociate from the cell cortex (41). In *Drosophila* placode border, aPKC phosphorylates Rok to deactivate its role in recruiting myosin (42). Based on these, Rok is a strong candidate as the myosin regulator during DC. To be prudent, however, we will use a generic name Reg in the model.

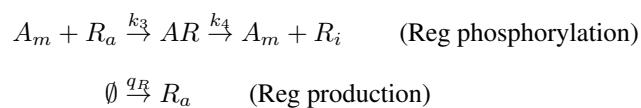
Another important feature of Fig. 1(b) is the localization and translocation of aPKC and Baz. At the onset of DC, the kinase-active store of aPKC is mostly bound to the plasma membrane to either of the two membrane proteins Cdc42 or Crumbs (47). As aPKC is prevented from accumulating on the basolateral plasma membranes by a molecular exclusion mechanism

(47), it has been observed mostly on the apical surface, and concentrated along the circumference (7, 15). Meanwhile, Baz is also concentrated in the adherens junctions in the apico-circumference region (47). During DC, the circumferential aPKC and Baz are progressively recruited to the apicomedial domain (15). More specifically, aPKC is recruited by the actomyosin network, and it in turn recruits Baz. Both proteins form puncta in the apicomedial region of the cell. Schematically, Fig. 1(b) uses two arrows to represent these two successive recruitments:



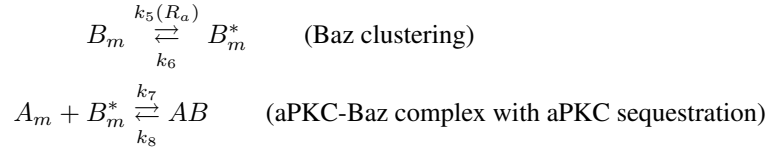
where we indicate both the rate constant and the recruiting agent for each migration. The exact mechanisms of the circumference-to-apicomedial translocation are unknown at present, although several possibilities, e.g. diffusion through the cytosol, direct translocation of large protein complexes along the membrane, and actomyosin advection, have been suggested based on *C. elegans* data (43–45). To account for the multiple steps involved in this process that are not explicitly modeled, we introduce a time delay  $\tau$  in converting the circumferential aPKC  $A_c$  to the medial aPKC  $A_m$ . For the transport of Baz, on the other hand, we do not implement an explicit delay. As explained below,  $B_m$  undergoes an oligomerization into a clustered form before its interaction with  $A_m$ . This two-step process will be modeled explicitly, with kinetic rates that amount to an effective delay that allows  $A_m$  the time to inactivate  $R_a$ . Besides, the Baz clusters have such a high capacity of sequestering aPKC that only a small fraction of  $B_c$  will have translocated medially (Fig. S8b in SM). Thus a further delay matters little to the model prediction. This is confirmed by numerical tests (Fig. S9).

Once medial, the PAR-proteins undergo a series of dynamic interactions that eventually leads to the cyclic assembly and disassembly of the medial actomyosin network in each AS cell. Medial aPKC inhibits actomyosin contraction by binding with an active form of Reg ( $R_a$ ) followed by a phosphorylation event and a quick unbinding, yielding an inactive form of Reg ( $R_i$ ) and the original aPKC molecule (41, 42):



We neglect specific reactivation of the inactive form of Reg ( $R_i$ ) into the active form  $R_a$ , and instead account for such reactivation through a Reg source  $q_R$ . This is motivated on the one hand by observations that an expression of upstream actomyosin regulators, e.g. DRhoGEF2 acting on Rho1 for downstream activation of Rok or Diaphanous (16), is necessary to maintain wild-type AS cell behavior. On the other hand,  $q_R$  also enables the model to predict a rising level of apicomedial myosin in later stages of DC, which is a prominent feature *in vivo*, both at the protein level (7, 15) and at the level of induced gene expression in the tissue (48).

The apicomedial Baz molecules ( $B_m$ ) become clustered ( $B_m^*$ ) under the influence of  $R_a$ . Imaging evidence suggests that this occurs through the mechanical tension produced by the actomyosin networks rather than chemical binding to the actomyosin; the tension may enhance Baz oligomerization through structural reorganization of the multi-domain protein (43, 49). The Baz clusters  $B_m^*$  then sequester  $A_m$  and antagonize its effect on myosin regulation (15, 43–45):



These reactions are indicated respectively by pointed and blunted arrows in Fig. 1(b). The sequestration of aPKC by Baz clusters has an uncertain stoichiometry. It is known that each Baz protein has multiple binding sites for the Par-6-aPKC complex (15, 50). Depending on the number of Baz in the cluster, each cluster can potentially sequester a large number of aPKC molecules before it is saturated. For lack of quantitative knowledge of the stoichiometry, we have made the simplifying assumption that a Baz cluster, once formed, can continue to sequester aPKC without being saturated. As will be seen later, this affects the model only in one minor aspect: the consumption of Baz in the medial domain.

The interactions described above establish a competition for  $A_m$  by  $R_a$  and  $B_m^*$ , and a potential scheme for generating a delayed negative feedback loop as hypothesized by David et al. (15). On reaching the apicomedial domain,  $A_m$  antagonizes  $R_a$  and causes the actomyosin network to disassemble. But  $A_m$  also recruits  $B_m$  to the medial domain, where  $B_m$  clusters into an agent that inhibits  $A_m$ , giving  $R_a$  the time to accumulate and reassemble the actomyosin network. The inhibition of  $A_m$  by  $B_m^*$  is helped by the fact that the dissociation rates  $k_6$  for  $B_m^*$  and  $k_8$  for  $AB$  are both slow, making  $B_m^*$  a potent aPKC sequestration mechanism (43–45). The transport and kinetic processes can be described by the following coupled differential equations, all protein species being expressed in terms of concentration:

$$\frac{dA_c}{dt} = -k_1 A_c R_a \quad (1)$$

$$\frac{dB_c}{dt} = -k_2 A_m B_c \quad (2)$$

$$\frac{dA_m}{dt} = k_1 A_c (t - \tau) R_a (t - \tau) - k_3 A_m R_a + k_4 AR - k_7 A_m B_m^* + k_8 AB \quad (3)$$

$$\frac{dB_m}{dt} = k_2 A_m B_c - k_5 B_m R_a + k_6 B_m^* \quad (4)$$

$$\frac{dR_a}{dt} = q_R - k_3 A_m R_a \quad (5)$$

$$\frac{dAR}{dt} = k_3 A_m R_a - k_4 AR \quad (6)$$

$$\frac{dR_i}{dt} = k_4 AR \quad (7)$$

$$\frac{dB_m^*}{dt} = k_5 B_m R_a - k_6 B_m^* \quad (8)$$

$$\frac{dAB}{dt} = k_7 A_m B_m^* - k_8 AB \quad (9)$$

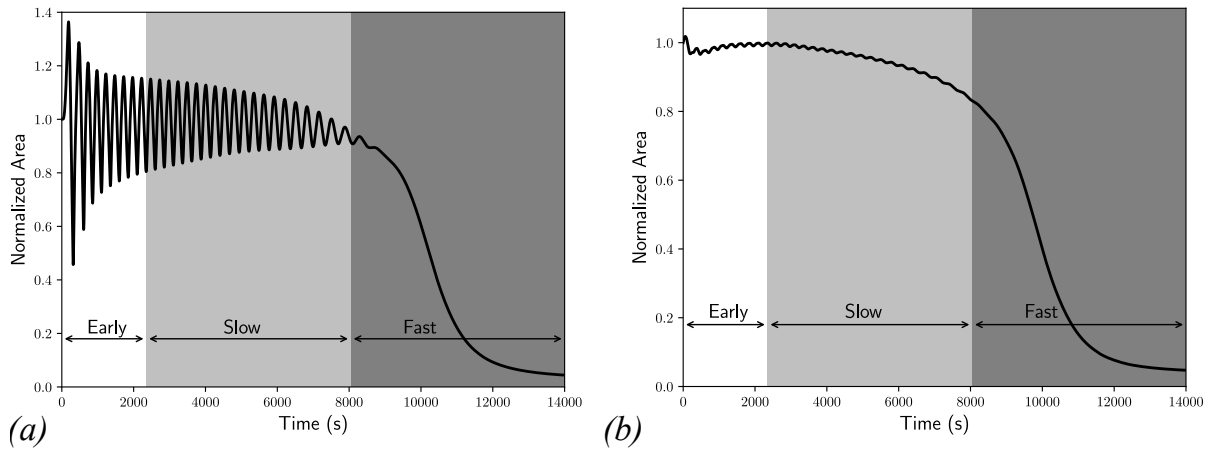


Figure 2: The temporal evolution of (a) the area of the representative cell of Fig. 1 and (b) the entire tissue area. Both areas are normalized by their initial values. The early phase shows oscillatory behavior, the slow phase shows dampening oscillations and gradual area loss, and the fast phase shows persistent loss of area.

The regulator  $R_a$  serves as the link between the kinetics of the biochemistry and the mechanics of actomyosin contraction. The scheme of distributing  $R_a$  in each cell among the six spokes and the kinetic equation for the attachment and detachment of myosin motors are the same as in Wang et al. (22), and details are given in the SM, Sec. S1. The model has a number of parameters, which are evaluated from experimental data where possible. To address uncertainties in the parameter values, we have performed a sensitivity analysis and found the kinetic model to be robust around the chosen values. Details of this analysis, along with a table of the parameter values, can be found in the SM, Sec. S2.

We start the simulation with an initial circumferential aPKC store of  $A_c$  and Baz store of  $B_c$ , and no Reg or myosin in the medial region. In the real amnioserosa, the cells exhibit phase lags among the neighbors and they oscillate preferentially in antiphase (1). To introduce the phase lag, we stagger the start of the kinetic model among the cells by a time randomly chosen between  $t = 0$  and  $t = T$ , where  $T \sim 260$  s is the period of oscillations observed in experiments (1) and also captured by our simulation.

## RESULTS

Our model is able to predict the three distinct phases of dorsal closure. Figure 2 depicts the temporal evolution of the area of a representative cell in panel (a) and that of the whole tissue in panel (b). The early phase features an oscillating tissue area without a sustained decrease over the cycles. This gives way to the slow phase that starts with the onset of net tissue area loss and ends with the cessation of oscillation on the cell level. The total loss in tissue area amounts to about 18% during the slow phase. Finally, the fast phase is distinguished by mostly monotonic shrinking of cell area and a rapid contraction of the tissue area toward closure. The dynamics of the entire process can be viewed in Movie S1 of the online SM. In the following we explore the molecular mechanisms that underlie each phase and trigger the transition from one to the next.

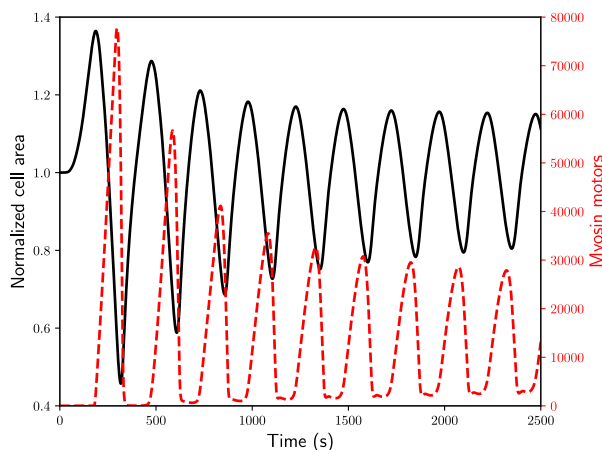


Figure 3: Early phase dynamics of the normalized area of the representative cell (black solid line) and the total myosin inside the cell (red dashed line).

### Early Phase: Oscillations

The purpose of this subsection is to investigate the origin of the oscillatory behavior of the AS cells within the context of the chemical signaling pathways detailed in the kinetic model. Figure 3 shows the early-phase dynamics of the myosin motors and cell area of the representative cell highlighted in Fig. 1(a). For this cell, the PAR-protein kinetics onset at  $t = 179$  s, before which the cell is only subject to mechanical forces from its neighbors, which cause the initial increase in its area. Once the biochemical network is activated, cell behavior becomes dominated by the internal myosin dynamics (see discussion of Fig. S6 in Sec. S3). Persistent oscillations of the cell area and the myosin level develop in time. The mean period of oscillations  $T \approx 260$  s matches experimental observations (1, 4). Parametric studies show that  $T$  is not very sensitive to the kinetic rate parameters (Figs. S1, S2), but it increases with  $\tau$  (Fig. S3). Within the context of the model, this suggests that the period of oscillations is an outcome of the transport and activation mechanisms of apicomedial aPKC. Moreover, the cell area oscillates roughly in anti-phase with the myosin, with an amplitude of about 20% among AS cells (Fig. 3). The maximum of myosin precedes the minimum of the cell area slightly, in agreement with experimental observations (4, 7, 22). The delay in the cell contraction is due to viscous damping. We have also calculated the cross correlation of the area change between neighboring cells. Although the cells have been given a random initial phase lag, once they settle into a regular oscillation, the mechanical coupling among neighbors produce on average a negative correlation (Fig. S6a), again in agreement with experimental observations (1, 4).

The area of the entire tissue also exhibits temporal variations (Fig. 2b, Movie S1), but the overall change is less than 6% during the early phase. As the actomyosin network is activated throughout the AS cells, the tissue area first declines by about 5% and then recovers to roughly its initial area. The decline is owing to the fact that the first few cycles of myosin oscillation are particularly strong, with large amplitudes (see Fig. 4a below). In time, it settles into a milder oscillatory pattern, producing the recovery in tissue area. This process manifests itself in the evolution of individual cell areas by a decrease in the amplitude

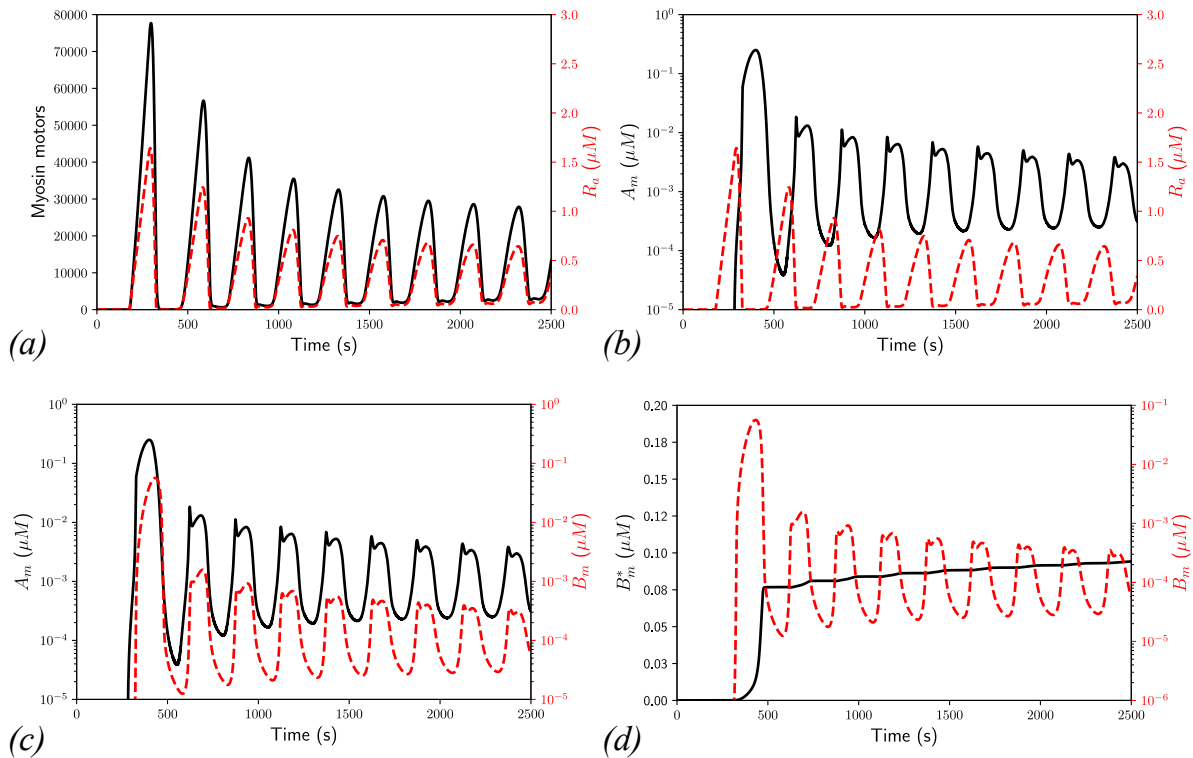


Figure 4: Evolution of various medial proteins in the representative cell during the early phase. (a) Number of myosin motors (black) and concentration of the actomyosin regulator  $R_a$  (red dashed). (b)  $R_a$  (red dashed) and its antagonist aPKC  $A_m$  (black). (c)  $A_m$  (black) and Baz  $B_m$  (red dashed). (d) Baz cluster  $B_m^*$  (black) and  $B_m$  (red dashed).

of the area (Fig. 2a). One can also discern small-amplitude oscillations in the whole tissue area, a collective effect of the oscillation of all the AS cells. In addition, we see little difference in behavior between the leading edge cells and those in the interior (Fig. S10).

Under the assumptions of the model, the origin of the oscillation can be sought from the temporal and spatial relationship among the PAR proteins and the regulator. The direct cause for the myosin pulse is a pulse in  $R_a$  (Fig. 4a).  $R_a$  grows because of the steady production  $q_R$  (Eq. 5), and its growth recruits  $A_m$  with a delay  $\tau$  (Eq. 3). As  $A_m$  accumulates in the apicomedial domain, it continues to phosphorylate and deactivate  $R_a$ , causing the latter to peak and then sharply decline (Fig. 4b). Thus, the medial myosin network disassembles as a result of the medial aPKC (7). Meanwhile,  $A_m$  recruits Baz (Eq. 4) so  $B_m$  rises in tandem with  $A_m$  (Fig. 4c). As  $B_m$  oligomerizes into  $B_m^*$  (Fig. 4d), the latter grows and in turn sequesters  $A_m$ , causing  $A_m$  to decline. With the now depressed level of  $A_m$ ,  $R_a$  is able to recover and re-assemble the actomyosin network, which sets up the next cycle of oscillation. The duration of the actomyosin contraction depends on how long  $A_m$  persists with Baz. Higher Baz prolongs the contraction phase as observed by David et al. (7).

It is interesting to note that the amplitude of the oscillation gradually declines in time for all proteins. The first few cycles have particularly large amplitudes. This is related to our model assumptions that initially all aPKC and Baz are stored in the

circumference of the cell's apical surface, and that the rate of recruitment to the medial domain is proportional to the entire stores of  $A_c$  and  $B_c$  (Eqs. 1, 2). Thus, the first few large waves are incidental to the setup of the simulation and practically inconsequential. However, a more consequential feature is that the circumferential stores of aPKC and Baz are finite and decline in time as more of them translocate to the apicomedial domain to mediate the actomyosin dynamics. We will return to the temporal decline of the amplitudes when discussing the transition to the slow and fast phases.

Thus, the model explains the oscillatory behavior of the AS cells from the *cell-autonomous* kinetics of signaling proteins involved in DC. The question of whether cell oscillation arises from intracellular or intercellular mechanisms has been debated in the literature. Some mathematical models, including the present model and that of Machado et al. (11), can produce oscillation from cell-autonomous mechanisms, while others rely on mechanical coupling between neighbors (1, 22). There is little doubt that the contractile phase of the oscillation is due to myosin motors inside each cell. It is the expansion phase that is in question. Experiments using holographic laser microsurgery (34) suggest that cell expansion is driven by intracellular forces, and is thus cell-autonomous. More recent data (12) paint a subtler picture in which a combination of autonomous and non-autonomous mechanisms drive cell expansion during AS oscillation. In our model, expansion occurs via passive elasticity of the cell, whose structural basis must be the actomyosin cortex. In this sense, our model is consistent with the cell-autonomous expansion noted by Hara et al. (12). But it does not discount an alternative pathway to oscillation through cell-cell coupling, which may coexist and cooperate with the cell-autonomous pathway in the real amnioserosa.

To sum up this subsection, our model is closely based on the observed intracellular kinetics of PAR proteins during DC (7, 15) and their effects on actomyosin observed in *Drosophila* and other organisms (41, 42). The possibility of aPKC phosphorylating Reg and complexing Baz results in a competition between the latter two, and sets up negative feedback from aPKC onto actomyosin and from Baz onto aPKC. Thus the oscillation arises in our model. By encoding the biological insights into a quantitative form, the model demonstrates a cell-autonomous mechanism for the oscillation.

### **Slow Phase: Ratcheting**

The beginning of the slow phase is defined as the onset of net contraction of the AS tissue (3, 4). In Fig. 2(b), we identify this as the instant  $t = 2352$  s when the tissue area reaches a maximum before starting to decline. The end of the slow phase is marked by the cessation of cell area oscillation and a dramatic acceleration of AS contraction rate (4). Using the data of Blanchard et al. (4) as a reference and considering the variation among our model cells, we have determined the end of the slow phase at  $t = 8046$  s, giving the slow phase a duration of 5694 s or roughly 95 min. Overall the slow phase is characterized by a gradual intensification of net area contraction. Measured by its maximum area in each cycle, our representative cell of Fig. 2(a) loses about 0.5% of area per cycle at the start, up to 3% per cycle toward the end, for a cumulative reduction of 20% during the slow phase. There is also a dampening of the amplitude of areal oscillation; it decreases from roughly 20% of the mean area to about 2% for the representative cell.

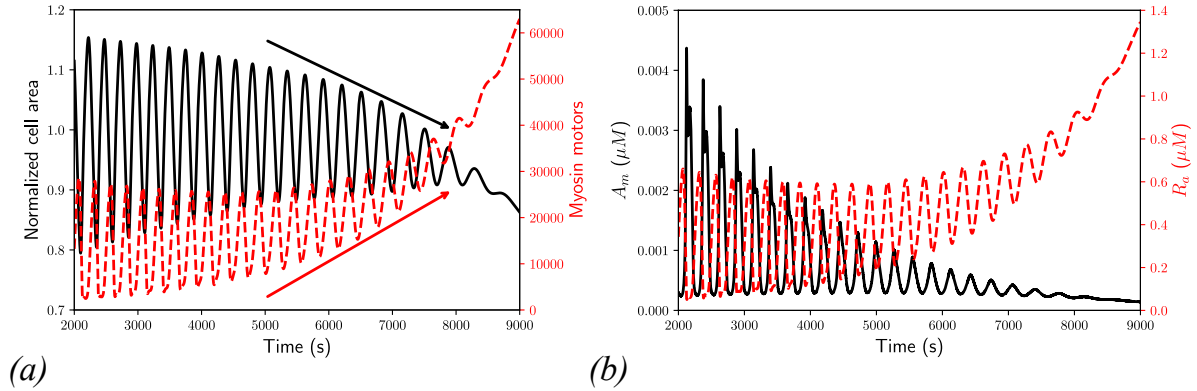


Figure 5: Evolution of various proteins in the representative cell during the slow phase. (a) Over each cycle of oscillation, an increase in myosin (red dashed) leads to constriction of the cell area (black), resulting in a ratchet-like effect. (b) The active Reg  $R_a$  (red dashed) rises over each cycle as the medial aPKC  $A_m$  (black) declines.

Our model captures the net decrease of cell area through an increasing average myosin level. This is evident from the temporal evolutions of both in the slow phase (Fig. 5a). With each cell cycle, the minimum myosin level increases (red arrow); it stabilizes the cell cortex and prevents the cell from relaxing to its original area (black arrow). Tracing the biochemistry upstream, the increasing myosin level is the result of a gradually rising  $R_a$ , which in turn is due to its source  $q_R$  and a decline in the level of apicomedial aPKC  $A_m$  (Fig. 5b). As we have started with a finite reservoir of circumferential aPKC,  $A_c$ , the total amount of  $A_m$  is also finite. As more of it is sequestered by  $B_m^*$ , there is progressively less available  $A_m$ . As a result,  $R_a$  rises over each cycle.

A central concept in the current view of cell constriction is the internal ratchet (1, 10, 14, 23). However, there is no convincing model or explanation of its underlying mechanism. The current hypothesis is that the cell cortex and internal actomyosin network stabilize themselves at the conclusion of every myosin pulse, thus preventing the cell area from returning to the previous value before the contraction (10, 14, 20). Then what stabilizes the actomyosin after each contractile pulse? Why is this behavior unique to the slow phase of DC, but not present in the oscillatory early phase? In their DC model, Wang et al. (22) addressed this by prescribing an *ad hoc* “mechanical ratchet”, reducing the resting length of each cell edge and spoke by a prescribed amount during the slow and late phases. Our model answers these questions on the basis of the biochemistry of the PAR proteins. During the early phase, there is still sufficient aPKC to antagonize the actomyosin regulator and allow the actomyosin network to disassemble. Consequently, the cell relaxes to its original area. The early phase comes to an end with the gradual exhaustion of apicomedial aPKC. In the slow phase, the declining level of aPKC is such that it is no longer able to completely suppress net myosin production in each cycle, resulting in a cumulative increase in the number of myosin motors with each successive cycle. This, our model suggests, is the molecular basis for the function of the actomyosin ratcheting.

The area of the entire AS tissue also shrinks gradually (Fig. 2b), the contraction amounting to roughly 18% by the end of the slow phase. Experimentally, the beginning of the slow phase has been observed to coincide with the formation of the

supracellular actin cable surrounding the AS tissue (3, 4), suggesting a major role for the actin cable in AS contraction (1, 3, 4). Follow-up studies concluded, however, that the actin cable is not the main cause of closure (9, 23, 24), and contributes only a small fraction of the total area loss (22). Considering its relatively minor role, we have chosen to model the actin cable *ad hoc* at a coarser level than the intracellular dynamics (details in Sec. S1 of SM). Our model predictions confirm the insignificance of the actin cable to dorsal closure (details in Sec. S4 of SM).

We close this subsection by noting two experimental features that the model fails to reproduce. First, Solon et al. (1) reported that the cessation of cell oscillation occurs first at the boundary with the epidermis, and propagates inward toward the midline of the AS. In our model, all cells display roughly the same amplitudes of oscillation as the PAR-protein dynamics are largely cell-autonomous. Thus, the cessation of oscillation occurs randomly throughout the tissue, depending on the initial phase lag among the cells and their mechanical coupling. Second, *in vivo* the amplitude of the oscillation dampens and its period shortens as the slow phase progresses (4). Our model captures the dampening of the oscillation due to the gradual buildup of apicomerial myosin, but not the reduction in the period  $T$ . Our period actually lengthens, from about 260 s at the start to 350 s toward the end (Fig. 2a). Evidently, our mathematical description of the PAR-proteins misses some subtle mechanism that shortens the oscillation period *in vivo*. In the model of Machado et al. (11), AS cell oscillation arises from the cyclic actin turnover, and these authors were able to produce a shortening period by prescribing an actin turnover rate that increases in time. But at present it is unclear what upstream mechanism could accelerate the actin turnover rate.

### Fast Phase: Closure

The fast phase, as observed *in vivo*, introduces two new factors into the closure of the AS tissue. The first is zippering (25–27), which occurs when filopodia are extended from one epidermis to the other and exert a pulling force to move the two leading edges toward each other. We have chosen to exclude this factor from the model because it is non-essential for dorsal closure (9) and is largely independent of the AS contraction. The second is apoptosis and delamination of AS cells (3, 8, 28), which mainly occurs at the canthi during the onset of the zippering process and contributes to the speed of dorsal closure. We model this process by eliminating a cell when its area falls below a threshold area ( $1 \mu\text{m}^2$ ) and all its edges are shorter than  $0.5 \mu\text{m}$  (Fig. S11). To maintain the integrity of the model tissue, we then collapse the outer nodes of the “apoptotic” cell onto the central node, a treatment motivated by *in vivo* experiments of Toyama et al. (28) and their Figure 2(a,b). If eliminating a cell brings the opposing epidermis together, we consider this the fusion of the epidermis and subsequently fix the location of the central node. This mimics the restructuring process that occurs at the canthi *in vivo* (9).

Upon the onset of the fast phase, the AS cells stop oscillating and undergo persistent constriction while the tissue area drops precipitously (Fig. 2b). The rapid loss of AS area lasts about 4000 s, as the rate of contraction slows down. It takes roughly another 2000 s of slow contraction to reduce the AS areas to below 5% of its initial value. This is considered “full closure” in our model, considering the lack of zippering. This duration of the fast phase is consistent with experimental observations (8, 29). Movie S1 in the online SM gives an overall view of the whole process.

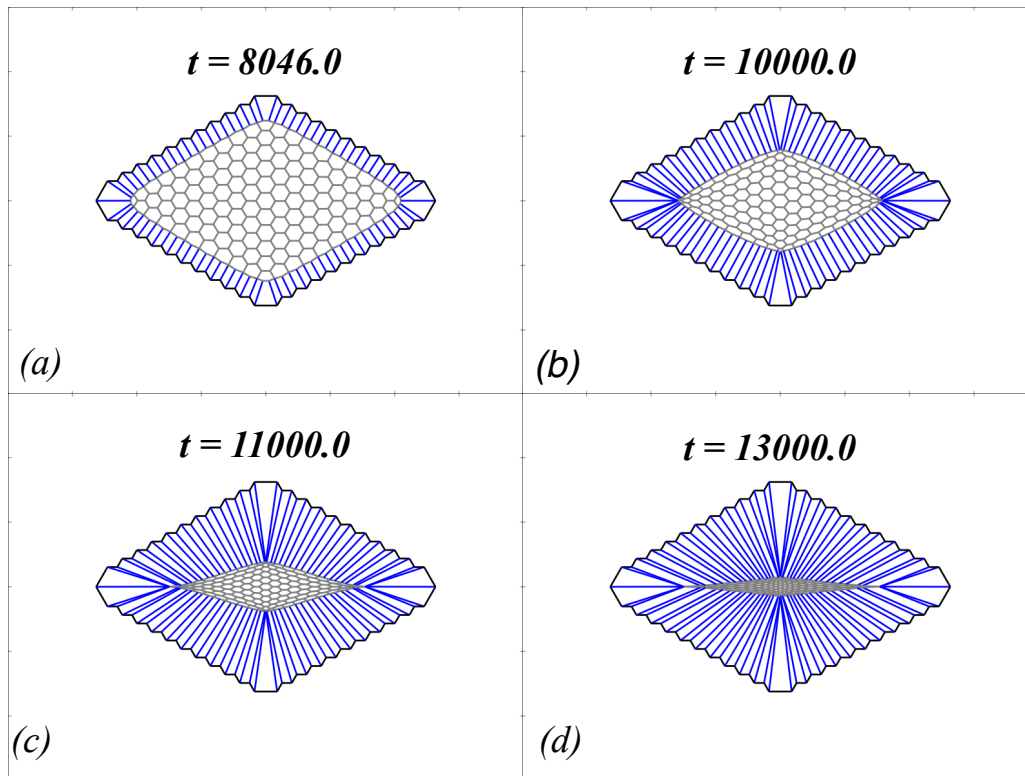


Figure 6: Contraction of the amnioserosa in the fast phase. (a) At the start of the fast phase  $t = 8046$  s, the tissue boundary has been smoothed by the actin cable as compared to the initial configuration. (b) Shortly before the canthi form around  $t = 10100$  s. (c) After canthi formation, the AS narrows rapidly in the medial-lateral direction. (d) At  $t = 13000$  s, the tissue area has fallen below 5% of its initial value, and this is considered full closure in the context of our modeling.

The evolving geometry of the amnioserosa is depicted in Fig. 6. At the start of the fast phase ( $t = 8046$  s), the geometry of the AS tissue resembles that of a rounded rhombus (Fig. 6a). As contraction becomes more intense, the outermost cells on the anterior-posterior axis are the first to become eligible for apoptosis (Fig. 6b). Their elimination forms two canthi around  $t = 10100$  s. Once the canthi fix the length of the AS tissue, it narrows rapidly into a spindle shape (Fig. 6c) that closely resembles the *in vivo* observation (9). In time, our AS tissue is able to shrink its area to below 5% of the initial value, producing a thin slit between the two epidermal tissues (Fig. 6d). This is the final “fully closed” geometry. Closure is a robust prediction of our model that is attained with and without the actin cable (Fig. S7), and over wide ranges of the kinetic parameters (see parametric study in Sec. S2 in SM).

What triggers the transition from the slow to the fast phase is the exhaustion of apicomedial aPKC. This is consistent with experimental observations of increased sequestration of aPKC by Baz in late DC (15, Fig. 5). Through the cycles of actomyosin assembly and disassembly of the early and slow phases, most of the circumferential aPKC ( $A_c$ ) has translocated to the medial domain, and the medial aPKC ( $A_m$ ) is gradually sequestered by  $B_m^*$ . Figure 7(a) shows the declining amplitude and mean of  $A_m$  in the early and slow phases, as each cycle receives less influx of aPKC from the circumferential  $A_c$ . Since  $B_m$  is recruited by  $A_m$  to the apicomedial domain, it follows a similar trend of decline. By the end of the slow phase,  $A_m$

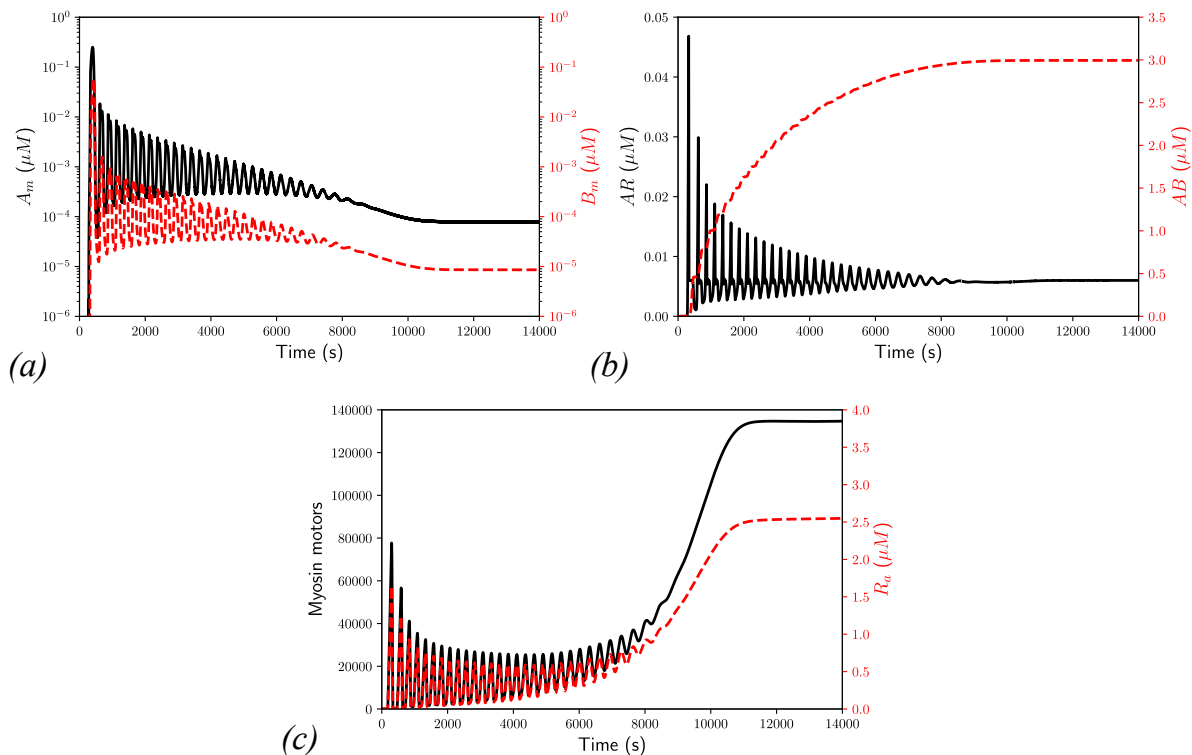


Figure 7: Dynamics of the key proteins in the representative cell explain the transition into the fast phase. (a)  $A_m$  (black) and  $B_m$  (red dashed) decline, as medial aPKC is consumed by phosphorylation of Reg and Baz. (b) The products  $AR$  (black) and  $AB$  (red dashed) attain a steady state in time. (c) Oscillations in myosin (black) and  $R_a$  (red dashed) in the slow phase give way to monotonic growth in the fast phase.

and  $B_m$  have more or less approached a steady state, as do the products  $AB$  and  $AR$  (Fig. 7b). Henceforth,  $A_m$  and  $B_m$  have essentially dropped out of the negative feedback that antagonizes  $R_a$  and suppresses the assembly of myosin. This triggers the transition into the fast phase as the myosin pulsation gives way to a monotonic rise (Fig. 7c), and the cell-area oscillation to persistent constriction. Note that the steady-state  $B_m$  concentration is considerably lower than that of  $A_m$ . This observation is consistent with experimental observations of less Baz than Par-6 in the apicomedial complexes (15).

Interestingly, we find that the circumferential Baz store  $B_c$  has little effect on the onset of the fast phase. While the entire circumferential store  $A_c$  is eventually recruited by Reg to the apicomedial region, the same is not true for  $B_c$  (Fig. S8). As  $A_m$  declines in the fast phase by way of Baz sequestration (Fig. 7a), so does its ability to effectively recruit Baz from the periphery to the medial domain. Thus, the transport of  $B_c$  to  $B_m$  dies out, with only about 4% of  $B_c$  having reached the apicomedial domain. Such a low level of apicomedial Baz is sufficient to carry out its task of sequestering aPKC, partly because of our assumption of  $B_m^*$  not being saturated in its capability of sequestering aPKC (Eq. 8). Biologically, the rationale is that the Baz cluster  $B_m^*$  has multiple binding sites for aPKC, and thus is not rendered ineffectual after forming the first complexes with aPKC (15, 39, 50, 51). Nevertheless, the large initial store of  $B_c$  is necessary for the early and slow phase. Our kinetics

is such that the rate of Baz migration is proportional to  $B_c$ . Thus, the large  $B_c$  maintains a sufficient rate of  $B_m$  that is needed for suppressing aPKC and allowing the actomyosin to reassemble.

Experimental consensus is that in the fast phase the PAR-proteins progressively accumulate apicomediaally and the actomyosin network becomes more persistent and pervasive throughout the AS tissue (15, 26). These observations guided the construction of the mathematical model described in Eqs. (1–9), and are recapitulated by our simulation results. The strengthened actomyosin network dampens the AS cell oscillations and effects persistent constriction (1, 4). Our model has predicted a natural transition from the slow to the fast phase, and also captured its key features noted above. In this regard, it marks an advance beyond previous modeling, which has rarely dealt with the fast phase (1, 11, 34, 35). An earlier model from our group (22), for example, was unable to predict the upsurge of apicomedial myosin in the fast phase. There was no chemical or mechanical cue to trigger the transition from oscillatory to non-oscillatory dynamics in the apicomedial myosin dynamics. In its stead, a mechanical ratchet was employed, by reducing the rest length of the edges and spokes in time, to produce rapid closure of the tissue.

## DISCUSSION

The objective of this work is to integrate experimental findings of the molecular signaling pathways in *Drosophila* dorsal closure into a quantitative and predictive model. The model has two key components. One is a PAR-protein regulatory circuit that has been suggested by recent observations (15, 39, 43–45). The other is a vertex-based cell mechanics model that is driven by myosin contraction. The myosin activation by a regulator downstream of the PAR-kinetics provides the linkage between the two. The model parameters have been evaluated based on available data, and the robustness of the results has been tested by varying these parameters. The main results of the paper consist of the following:

- The model predicts the oscillations in the apical area of amnioserosa cells in the early phase, and provides an explanation for it from the cell-autonomous biochemistry of the PAR proteins.
- The model predicts the internal ratchet that causes gradual loss of cell area in the slow phase of dorsal closure, and explains its molecular mechanism based on the same biochemistry.
- The model predicts the cessation of cellular oscillation in the fast and final phase of dorsal closure, as well as the rapid and persistent contraction of cell and tissue area, again from the biochemistry.

The model predictions are in reasonable agreement with experiments. For example, it reproduces the various time scales of the process, including the period of oscillation and the duration of the three phases, confirms the anti-phase correlation among neighbors and the minor role of the supracellular actin cable, and recapitulates the temporal dynamics of the key proteins, especially the intensification of apicomedial myosin in the later stage of dorsal closure. Therefore, from a minimal regulatory circuit and cell mechanics, the model is able to capture most key features of the experimental observations in the early, slow

and fast phases, as well as the transition among them. It provides a coherent framework that connects the tissue- and cell-level events to the intracellular transport and interaction of the PAR proteins. These are the main contributions of the current work.

Of the factors contributing to dorsal closure, we have accounted for the intracellular contraction of actomyosin, the supra-cellular actin cable, the interaction with the surrounding epidermis, and the delamination of apoptotic cells. Zippering, an important mechanism during the final stage of closure, has been neglected completely. Of the factors included, the actomyosin contraction is modeled with the greatest care; it is the centerpiece of the model. The three other factors are modeled more *ad hoc*, using convenient mechanical and mathematical constructs. This is partly for lack of an understanding of the underlying mechanisms, and partly for their secondary roles in the dorsal closure process. As more is learned about them, the new knowledge can be used to refine the modeling. The model predicts the oscillatory dynamics of the early phase from a cell-autonomous mechanism. This leaves aside, but by no means discounts or disproves, potential roles of cell-cell coupling. Mechanical coupling occurs through forces and deformation, as accounted for by earlier models (1, 22). There may also be biochemical coupling, as evidenced by the intriguing phenomenon of an actomyosin pulse propagating between neighbors (7). This suggests potential pathways through cadherin-based mechanobiology at cell junctions (52, 53), or through mechanically gated ion channels (54).

Of necessity, the model makes simplifying assumptions about a complex biological process, and omits some of its less important elements. A key assumption is a steady source for the actomyosin regulator  $R_a$ , as this lies at the root of the ratcheting and rapid closure in the last two phases. The identity of this regulator has been discussed by several groups (15, 17, 40–42), and Rho kinase appears as a highly plausible candidate among several hypothesized. An obvious task for future experiments is to identify the regulator unambiguously. The assumption of its source and continual supply is also testable in future experiments, by examining its gene expression and medial protein levels in relation to upstream regulators and downstream contractile myosin networks. Besides, for lack of precise knowledge of the stoichiometry of aPKC sequestration by Bazooka clusters, we have assigned unsaturated binding capability to these clusters. An unrealistic consequence is the minimal re-localization of Baz from the circumference to the medial domain, in comparison to *in vivo* observations (e.g. Fig. 2 of David et al. (15)). Future experiments should investigate the complex formation between aPKC and Bazooka and gather quantitative data on the stoichiometry.

The most glaring failure of the model is that it predicts a lengthening period for the AS cell oscillation during the slow phase with internal ratcheting, whereas in reality the damping of the oscillation is accompanied by a shortening of the period (4). We can think of two potential causes for the discrepancy, one geometric and the other mechanical. As DC progresses, the shrinking cellular area should entail faster transport for the PAR proteins and potentially accelerate the downstream kinetics. This is unaccounted for in the model. Furthermore, experiments show that the tissue is under increasing tension during DC, and its mechanics changes from fluid-like to solid-like (15, 26, 35). The strengthening of the actomyosin and the rising tension have been captured by the model. However, this gradual rigidification does not translate to an increase in oscillation frequency, as one may expect based on mechanical intuition. The model determines the frequency of AS oscillation mostly

from the kinetics of the PAR proteins, and does not take adequate account of the rheological properties of the cells and tissue, including viscoelasticity (35). The various shortcomings of the model may motivate remedies and refinements in future work.

## AUTHOR CONTRIBUTIONS

TJCH and JJF designed the research project. CHD performed the numerical computations. All three authors contributed to the model formulation, data analysis, and the writing of the article.

## ACKNOWLEDGMENT

We acknowledge financial support by NSERC through Discovery Grant No. 05862 (to JJF) and No. 05617 (to TJCH). We thank William Lou and Amir Mafi for their contribution to an earlier version of the model, and Shane Hutson and Christoph Schmidt for discussions following the presentation of this work at the APS March Meeting in 2018.

## SUPPORTING CITATIONS

Reference (55–61) appear in the Supporting Material.

## References

1. Solon, J., A. Kaya-Çopur, J. Colombelli, and D. Brunner, 2009. Pulsed forces timed by a ratchet-like mechanism drive directed tissue movement during dorsal closure. *Cell* 137:1331–1342.
2. Ma, X., H. E. Lynch, P. C. Scully, and M. S. Hutson, 2009. Probing embryonic tissue mechanics with laser hole drilling. *Phys. Biol.* 6:036004.
3. Gorfinkiel, N., G. B. Blanchard, R. J. Adams, and A. Martinez Arias, 2009. Mechanical control of global cell behaviour during dorsal closure in *Drosophila*. *Development* 136:1889–1898.
4. Blanchard, G. B., S. Murugesu, R. J. Adams, A. Martinez-Arias, and N. Gorfinkiel, 2010. Cytoskeletal dynamics and supracellular organisation of cell shape fluctuations during dorsal closure. *Development* 137:2743–2752.
5. Saravanan, S., C. Meghana, and M. Narasimha, 2013. Local, cell-nonautonomous feedback regulation of myosin dynamics patterns transitions in cell behavior: a role for tension and geometry? *Mol. Biol. Cell* 24:2350–2361.
6. Kiehart, D. P., J. M. Crawford, A. Aristotelous, S. Venakides, and G. S. Edwards, 2017. Cell sheet morphogenesis: dorsal closure in *Drosophila melanogaster* as a model system. *Ann. Rev. Cell Dev. Biol.* 33:169–202.
7. David, D. J. V., A. Tishkina, and T. J. C. Harris, 2010. The PAR complex regulates pulsed actomyosin contractions during amnioserosa apical constriction in *Drosophila*. *Development* 137:1645–1655.
8. Sokolow, A., Y. Toyama, D. P. Kiehart, and G. S. Edwards, 2012. Cell ingression and apical shape oscillations during dorsal closure in *Drosophila*. *Biophys. J.* 102:969–979.
9. Wells, A. R., R. S. Zou, U. S. Tulu, A. C. Sokolow, J. M. Crawford, G. S. Edwards, and D. P. Kiehart, 2014. Complete canthi removal

- reveals that forces from the amnioserosa alone are sufficient to drive dorsal closure in *Drosophila*. *Mol. Biol. Cell* 25:3552–68.
10. Martin, A. C., M. Kaschube, and E. F. Wieschaus, 2009. Pulsed contractions of an actin-myosin network drive apical constriction. *Nature* 457:495–499.
  11. Machado, P. F., G. B. Blanchard, J. Duque, and N. Gorfinkiel, 2014. Cytoskeletal turnover and myosin contractility drive cell autonomous oscillations in a model of *Drosophila* dorsal closure. *Eur. Phys. J. Spec. Top.* 223:1391–1402.
  12. Hara, Y., M. Shagirov, and Y. Toyama, 2016. Cell boundary elongation by non-autonomous contractility in cell oscillation. *Curr. Biol.* 26:2388–2396.
  13. Munjal, a., and T. Lecuit, 2014. Actomyosin networks and tissue morphogenesis. *Development* 141:1789–1793.
  14. Munjal, A., J.-M. Philippe, E. Munro, and T. Lecuit, 2015. A self-organized biomechanical network drives shape changes during tissue morphogenesis. *Nature* 524:351–355.
  15. David, D. J. V., Q. Wang, J. J. Feng, and T. J. C. Harris, 2013. Bazooka inhibits aPKC to limit antagonism of actomyosin networks during amnioserosa apical constriction. *Development* 140:4719–4729.
  16. Azevedo, D., M. Antunes, S. Prag, X. Ma, U. Hacker, G. W. Brodland, M. S. Hutson, J. Solon, and A. Jacinto, 2011. DRhoGEF2 regulates cellular tension and cell pulsations in the amnioserosa during *Drosophila* dorsal closure. *PLoS ONE* 6:e23964.
  17. Wang, H. R., Y. Zhang, B. Ozdamar, A. A. Ogunjimi, E. Alexandrova, G. H. Thomsen, and J. L. Wrana, 2003. Regulation of cell polarity and protrusion formation by targeting RhoA for degradation. *Science* 302:1775–1779.
  18. Even-Faitelson, L., and S. Ravid, 2006. PAK1 and aPKCzeta regulate myosin II-B phosphorylation: a novel signaling pathway regulating filament assembly. *Mol. Biol. Cell* 17:2869–2881.
  19. Saias, L., J. Swoger, A. D’Angelo, P. Hayes, J. Colombelli, J. Sharpe, G. Salbreux, and J. Solon, 2015. Decrease in cell volume generates contractile forces driving dorsal closure. *Dev. Cell* 33:611–621.
  20. Martin, A. C., 2010. Pulsation and stabilization: Contractile forces that underlie morphogenesis. *Dev. Biol.* 341:114–125.
  21. Kiehart, D. P., C. G. Galbraith, K. A. Edwards, W. L. Rickoll, and R. A. Montague, 2000. Multiple forces contribute to cell sheet morphogenesis for dorsal closure in *Drosophila*. *J. Cell Biol.* 149:471–490.
  22. Wang, Q., J. J. Feng, and L. M. Pismen, 2012. A cell-level biomechanical model of *Drosophila* dorsal closure. *Biophys. J.* 103:2265–2274.
  23. Pasakarnis, L., E. Frei, E. Caussinus, M. Affolter, and D. Brunner, 2016. Amnioserosa cell constriction but not epidermal actin cable tension autonomously drives dorsal closure. *Nat. Cell Biol.* 18:1161–1172.
  24. Ducuing, A., and S. Vincent, 2016. The actin cable is dispensable in directing dorsal closure dynamics but neutralizes mechanical stress to prevent scarring in the *Drosophila* embryo. *Nat. Cell Biol.* 18:1149–1160.
  25. Millard, T. H., and P. Martin, 2008. Dynamic analysis of filopodial interactions during the zipper phase of *Drosophila* dorsal closure. *Development* 135:621–626.
  26. Gorfinkiel, N., S. Schamberg, and G. B. Blanchard, 2011. Integrative approaches to morphogenesis: Lessons from dorsal closure. *Genesis* 49:522–533.
  27. Lu, H., A. Sokolow, D. P. Kiehart, and G. S. Edwards, 2015. Remodeling tissue interfaces and the thermodynamics of zipping during dorsal closure in *Drosophila*. *Biophys. J.* 109:2406–2417.
  28. Toyama, Y., X. G. Peralta, A. R. Wells, D. P. Kiehart, and G. S. Edwards, 2008. Apoptotic force and tissue dynamics during *Drosophila*

- embryogenesis. *Science* 321:1683–1686.
29. Mateus, A. M., N. Gorfinkiel, S. Schamberg, and A. Martinez Arias, 2011. Endocytic and recycling endosomes modulate cell shape changes and tissue behaviour during morphogenesis in *Drosophila*. *PLoS ONE* 6:e18729.
  30. Almeida, L., P. Bagnerini, A. Habbal, S. Noselli, and F. Serman, 2011. A mathematical model for dorsal closure. *J. Theoret. Biol.* 268:105 – 119.
  31. Aristotelous, A., J. Crawford, G. Edwards, D. Kiehart, and S. Venakides, 2018. Mathematical models of dorsal closure. *Prog. Biophys. Mol. Biol.* 137:111 – 131.
  32. Layton, A. T., Y. Toyama, G. Q. Yang, G. S. Edwards, D. P. Kiehart, and S. Venakides, 2009. *Drosophila* morphogenesis: Tissue force laws and the modeling of dorsal closure. *HFSP J.* 3:441–460.
  33. Hutson, M. S., J. Veldhuis, X. Ma, H. E. Lynch, P. G. Cranston, and G. W. Brodland, 2009. Combining laser microsurgery and finite element modeling to assess cell-level epithelial mechanics. *Biophys. J.* 97:3075–3085.
  34. Jayasinghe, A. K., S. M. Crews, D. N. Mashburn, and M. S. Hutson, 2013. Apical oscillations in amnioserosa cells: Basolateral coupling and mechanical autonomy. *Biophys. J.* 105:255–265.
  35. Machado, P. F., J. Duque, J. Étienne, A. Martinez-Arias, G. B. Blanchard, and N. Gorfinkiel, 2015. Emergent material properties of developing epithelial tissues. *BMC Biol.* 13:98.
  36. Gorfinkiel, N., 2013. Mechano-chemical coupling drives cell area oscillations during morphogenesis. *Biophys. J.* 104:1–3.
  37. Harris, T. J. C., and J. J. Feng, 2014. Comment on Machado et al., “Cytoskeletal turnover and myosin contractility drive cell autonomous oscillations in a model of *Drosophila* dorsal closure”. *Eur. Phys. J. Spec. Top.* 223:1437–1439.
  38. Hutson, M. S., 2003. Forces for morphogenesis investigated with laser microsurgery and quantitative modeling. *Science* 300:145–149.
  39. Renschler, F. A., S. R. Bruekner, P. L. Salomon, A. Mukherjee, L. Kullmann, M. C. Schütz-Stoffregen, C. Henzler, T. Pawson, M. P. Krahn, and S. Wiesner, 2018. Structural basis for the interaction between the cell polarity proteins Par3 and Par6. *Sci. Signal.* 11:eaam9899.
  40. Zhang, H., and I. G. Macara, 2008. The PAR-6 polarity protein regulates dendritic spine morphogenesis through p190 RhoGAP and the Rho GTPase. *Dev. Cell* 14:216–226.
  41. Ishiuchi, T., and M. Takeichi, 2011. Willin and Par3 cooperatively regulate epithelial apical constriction through aPKC-mediated ROCK phosphorylation. *Nat. Cell Biol.* 13:860–866.
  42. Röper, K., 2012. Anisotropy of Crumbs and aPKC drives myosin cable assembly during tube formation. *Dev. Cell* 23:939–953.
  43. Wang, S.-C., T. Y. F. Low, Y. Nishimura, L. Gole, W. Yu, and F. Motegi, 2017. Cortical forces and CDC-42 control clustering of PAR proteins for *Caenorhabditis elegans* embryonic polarization. *Nat. Cell Biol.* 19:988–995.
  44. Dickinson, D. J., F. Schwager, L. Pintard, M. Gotta, and B. Goldstein, 2017. A single-cell biochemistry approach reveals PAR complex dynamics during cell polarization. *Dev. Cell* 42:416–434.e11.
  45. Rodriguez, J., F. Peglion, J. Martin, L. Hubatsch, J. Reich, N. Hirani, A. G. Gubieda, J. Roffey, A. R. Fernandes, D. St Johnston, J. Ahringer, and N. W. Goehring, 2017. aPKC cycles between functionally distinct PAR protein assemblies to drive cell polarity. *Dev. Cell* 42:400–415.e9.
  46. Graybill, C., B. Wee, S. X. Atwood, and K. E. Prehoda, 2012. Partitioning-defective protein 6 (Par-6) activates atypical protein kinase C (aPKC) by pseudosubstrate displacement. *J. Biol. Chem.* 287:21003–21011.

47. Tepass, U., 2012. The apical polarity protein network in *Drosophila* epithelial cells: Regulation of polarity, junctions, morphogenesis, cell growth, and survival. *Annu. Rev. Cell Dev. Biol.* 28:655–685.
48. Zahedi, B., W. Shen, X. Xu, X. Chen, M. Mahey, and N. Harden, 2008. Leading edge-secreted Dpp cooperates with ACK-dependent signaling from the amnioserosa to regulate myosin levels during dorsal closure. *Dev. Dyn.* 237:2936–2946.
49. Harris, T., 2017. Protein clustering for cell polarity: Par-3 as a paradigm [version 1; referees: 3 approved]. *F1000Research* 6:1620.
50. Morais-de Sá, E., V. Mirouse, and D. St Johnston, 2010. aPKC phosphorylation of Bazooka defines the apical/lateral border in *Drosophila* epithelial cells. *Cell* 141:509–523.
51. Wodarz, A., A. Ramrath, A. Grimm, and E. Knust, 2000. *Drosophila* atypical protein kinase C associates with Bazooka and controls polarity of epithelia and neuroblasts. *J. Cell Biol.* 150:1361–1374.
52. Hoffman, B. D., C. Grashoff, and M. A. Schwartz, 2011. Dynamic molecular processes mediate cellular mechanotransduction. *Nature* 475:316–323.
53. Hoffman, B. D., and A. S. Yap, 2015. Towards a dynamic understanding of cadherin-based mechanobiology. *Trends Cell Biol.* 25:803–814.
54. Hunter, G. L., J. M. Crawford, J. Z. Genkins, and D. P. Kiehart, 2014. Ion channels contribute to the regulation of cell sheet forces during *Drosophila* dorsal closure. *Development* 141:325–334.
55. Forgacs, G., R. A. Foty, Y. Shafir, and M. S. Steinberg, 1998. Viscoelastic properties of living embryonic tissues: A quantitative study. *Biophys. J.* 74:2227–2234.
56. Kovacs, M., K. Thirumurugan, P. J. Knight, and J. R. Sellers, 2007. Load-dependent mechanism of nonmuscle myosin 2. *Proc. Natl. Acad. Sci. U.S.A.* 104:9994–9999.
57. Besser, A., and U. S. Schwarz, 2007. Coupling biochemistry and mechanics in cell adhesion: A model for inhomogeneous stress fiber contraction. *New J. Phys.* 9:425.
58. Fernandez-Gonzalez, R., S. de Matos Simões, J.-C. Röper, S. Eaton, and J. A. Zallen, 2009. Myosin II dynamics are regulated by tension in intercalating cells. *Dev. Cell* 17:736–743.
59. Phillips, R., J. Kondev, J. Theriot, and H. Garcia, 2012. *Physical Biology of the Cell*. Garland Science.
60. Milo, R., and R. Phillips, 2015. *Cell Biology by the Numbers*. Garland Science.
61. Hayes, P., and J. Solon, 2017. *Drosophila* dorsal closure: An orchestra of forces to zip shut the embryo. *Mech. Develop.* 144:2–10.

# Supporting Material for “Dynamics of PAR proteins explain the oscillation and ratcheting mechanisms in dorsal closure”

C.H. Durney<sup>1</sup>, T.J.C. Harris<sup>2</sup>, J.J. Feng<sup>1,3</sup>

<sup>1</sup> Department of Mathematics, University of British Columbia, Vancouver, British Columbia, Canada

<sup>2</sup> Department of Cell & Systems Biology, University of Toronto, Toronto, Ontario, Canada

<sup>3</sup> Department of Chemical and Biological Engineering, University of British Columbia, Vancouver, British Columbia, Canada

## S1 Mechanical model

The structure of our model is such that the kinetics of the PAR proteins feed into the mechanics of the amnioserosa through the active form of the regulator  $R_a$ . Since  $R_a$  is defined for each cell while the apicomedial myosin is defined on the six spokes, we use a geometric factor  $h_{ij}$  to distribute  $R_a$  onto each of its spokes (1):

$$h_{ij} = \frac{\frac{1}{2}\text{area of } \triangle_{i,j-1,j} + \frac{1}{2}\text{area of } \triangle_{i,j,j+1}}{\text{area of cell}},$$

where the numerator is the average of the area of the two triangles on either side of the spoke  $ij$ . On each spoke, the number of active myosin motors varies according to  $R_a$ -induced attachment at rate  $k^+$  and spontaneous detachment at rate  $k^-$ :

$$\frac{dm_{ij}}{dt} = k^+ R_a h_{ij} - k^- m_{ij}, \quad (\text{S1})$$

where the myosin detachment is suppressed by tension, based on a well-established positive feedback loop (2, 3):

$$k^- = \begin{cases} c_1 e^{-c_2 f_{ij}}, & f_{ij} > 0 \\ c_1, & f_{ij} \leq 0 \end{cases}, \quad (\text{S2})$$

The mechanical framework is essentially the same as in the previous model of Wang et al. (1). The force on any given node  $i$  by adjacent node  $j$  is given by

$$f_{ij} = \mu(l_{ij} - l_0) + \beta m_{ij}, \quad (\text{S3})$$

where  $\mu$  is the elastic modulus,  $l_{ij}$  and  $l_0$  are the current length and the rest length of the cell edge or spoke,  $\beta$  is the force per myosin motor and  $m_{ij}$  denotes the number of myosin currently attached to a spoke. The sign convention is such that a positive

$f_{ij}$  indicates tension on the segment. There is always cortical myosin, of course. But since it plays no major role during DC, we have absorbed its contractile effect into the resting length  $l_0$  of an edge. Thus, only the apicomedial myosin is accounted for explicitly, and  $m_{ij} = 0$  on an edge. Tissue deformation is realized by the nodal motion governed by over-damped dynamics with a viscous friction factor  $\eta$ :

$$\eta \frac{d\mathbf{x}_i}{dt} = \mathbf{f}_i = \sum_j f_{ij} \frac{\mathbf{x}_j - \mathbf{x}_i}{|\mathbf{x}_j - \mathbf{x}_i|}, \quad (\text{S4})$$

where the force on the  $i^{\text{th}}$  node  $\mathbf{f}_i$  sums the forces  $f_{ij}$  on each segment connecting node  $i$  to an adjacent node  $j$ . Based on the characteristic velocity of cell contraction, we estimate, a posteriori, the Reynolds number of the cytoplasmic flow to be on the order of  $10^{-8}$ . Thus, the assumption of over-damped motion is fully justified. At the start of the simulation, there is no apicomedial myosin, and the initial length of the edges and spokes is such that the tissue is under an homogeneous tension (4).

The surrounding epidermis resists the dorsal closure (5, 6), but a detailed treatment of this resistance entails an account for the mechanics and structural remodeling of the epidermis (7). For simplicity and following prior modeling (4, 8), we use elastic tension lines to connect the outermost nodes of the AS tissue to a stationary outer boundary (blue lines Fig. 1a of the main text). These tension lines have the same elastic modulus  $\mu$  and resting length  $l_0$  as the edges and spokes in the interior, and initially carry a force that equals to the initial amnioserosa tension plus an extra tension  $F_c$ , the latter to anticipate the contraction of the tissue upon onset of medial myosin.

The supracellular actin cable forms on the interface between the epidermis and the AS. As the actin cable only plays a secondary role in the closure event (1, 9–11), we have elected to model it *ad hoc* by adding additional myosin along the outline of the AS tissue, i.e. through the outermost nodes (magenta in Fig. 1a of the main text):

$$m(t) = \begin{cases} 0, & t < t_0 \\ M \frac{t-t_0}{t_1-t_0}, & t_0 \leq t \leq t_1 \\ M, & t > t_1. \end{cases} \quad (\text{S5})$$

The piecewise linear form is motivated by recent *in vivo* imaging that suggests that the actomyosin in the actin cable increases roughly linearly during DC, saturating around 120 min (12, 13). The maximum  $M$  is chosen to be comparable to the maximum apicomedial myosin level during the early and slow phases. Although we know little of the signaling pathways upstream of the formation of the actin cable, the accumulation of myosin is likely through similar pathways to that of the cortical myosin and should be expressed at similar levels. The parameters  $t_0$  and  $t_1$  were chosen to match the curve presented in Fig. 2B of Hayes and Solon (13). Finally, we neglect zippering forces in our model. Although zippering is essential to the final fusing of the epidermis, it functions only at the end of the closure, and does not interact with the earlier dynamics on which this work focuses.

Table S1: Values of the parameters used in the model and their sources where available.

Parameters		Values	Sources	
Kinetic	aPKC migration	$k_1$	$0.00125 \mu\text{M}^{-1} \text{s}^{-1}$	
	Baz migration	$k_2$	$0.00125 \mu\text{M}^{-1} \text{s}^{-1}$	
	aPKC/Reg reaction	$k_3$	$2.5 \text{s}^{-1}$	
	aPKC/Reg unbinding	$k_4$	$75.0 \mu\text{M}^{-1} \text{s}^{-1}$	
	Baz clustering	$k_5$	$5.0 \mu\text{M}^{-1} \text{s}^{-1}$	
	Baz cluster dissociation	$k_6$	$0.001 \text{s}^{-1}$	
	aPKC sequestration	$k_7$	$3.5 \mu\text{M}^{-1} \text{s}^{-1}$	
	aPKC release	$k_8$	$0.00001 \text{s}^{-1}$	
	Reg production	$q_R$	$0.015 \mu\text{M} \text{s}^{-1}$	
	aPKC transport delay	$\tau$	100 s	
	myosin attachment rate	$k^+$	$10^4 \mu\text{M}^{-1} \text{s}^{-1}$	
	myosin detachment rate	$c_1$	$0.25 \text{s}^{-1}$	(2)
	tension-factor for myosin detachment	$c_2$	$1.33 \times 10^{-2} \text{nN}^{-1}$	
Mechanical	spoke elastic modulus	$\mu$	$0.75 \text{nN} \mu\text{m}^{-1}$	(4)
	spoke rest length	$l_0$	5.0 $\mu\text{m}$	(4)
	force per myosin motor	$\beta$	$10^{-3} \text{nN/motor}$	(14)
	viscous friction factor	$\eta$	100.0 $\text{nN s} \mu\text{m}^{-1}$	(15, 16)
	constant epidermal tension	$F_c$	5.0 nN	
Initial Condition	aPKC (circumferential)	$A_c$	3.0 $\mu\text{M}$	(17)
	Baz (circumferential)	$B_c$	3.0 $\mu\text{M}$	(17)
	all other proteins		0	
	spoke length	$l_{ij}$	7.6 $\mu\text{m}$	(4, 12, 18–20)
Actin Cable	maximum number of myosin	$M$	30000	
	initial onset	$t_0$	2700 s	(12, 13)
	time of saturation	$t_1$	9900 s	(12, 13)

## S2 Model parameters and sensitivity analysis

The model parameters are tabulated in Table S1 in four categories: kinetic parameters, mechanical parameters, initial conditions and parameters for the supracellular actin cable. The parameter values are estimated from the experimental literature where possible, and such sources are listed as well. If no reliable information is available, we have chosen values to produce desirable model predictions. To address such uncertainties in parameter evaluation, we have performed a sensitivity analysis by varying each of the uncertain parameters from its baseline value listed in the table and examining how the model prediction changes. The conclusion is that the qualitative features of the model predictions are robust and prevail over a reasonably wide range of parameters. Quantitatively, of course, the results do vary with each of the parameters with a different degree of sensitivity. In the following we present details of the sensitivity tests.

### S2.1 Kinetic parameters

This subsection focuses on the key kinetic parameters  $k_1, k_2, \dots, k_8, q_R$  and  $\tau$ . Parameters involved in the actin cable (see Eq. S5) will be discussed separately in Sec. S4 below. Starting with the baseline values of the kinetic parameters of Table S1, we vary each of these parameters to find an upper and lower bound outside of which at least one of the desirable features of

Table S2: The lower bounds for the kinetic parameters, given as multiplicative factors that, when multiplied by the baseline parameter values, yield the thresholds for each parameter.

Parameter	Baseline	Lower bound	Oscillations	Dampening	Ratchet	Fast Phase
$k_1$	0.00125	0.5	Yes	Yes	Yes	No <sup>1</sup>
$k_2$	0.00125	0.2	Yes	Yes	Yes	No <sup>1</sup>
$k_3$	2.5	0.1	Yes	No <sup>2</sup>	Yes	Yes
$k_4$	75	0.4	Yes	Yes	Yes	No <sup>3</sup>
$k_5$	5	0.05	Yes	Yes	Yes	No <sup>3</sup>
$k_6$	0.001	0 <sup>4</sup>	Yes	Yes	Yes	Yes
$k_7$	3.5	0.25	Yes	Yes	Yes	No <sup>1</sup>
$k_8$	0.00001	0	Yes	No <sup>5</sup>	Yes	Yes
$q_R$	0.15	0.75	Yes	Yes	Yes	No <sup>1</sup>
$\tau$	100	0.4	Yes <sup>6</sup>	Yes	Yes	No <sup>1</sup>

<sup>1</sup> Delayed onset of the fast phase.

<sup>2</sup> Increasing amplitude.

<sup>3</sup> Premature onset of fast phase.

<sup>4</sup>  $k_6 = 0$  yields nearly identical results to the baseline.

<sup>5</sup> No discernible dampening of oscillations before onset of fast phase.

<sup>6</sup> Period too short.

Table S3: The upper bounds for the kinetic parameters given as multiplicative factors.

Parameter	Baseline	Upper bound	Oscillations	Dampening	Ratchet	Fast Phase
$k_1$	0.00125	2.00	Yes	Yes	Yes	No <sup>1</sup>
$k_2$	0.00125	10.00	Yes	Yes	Yes	No <sup>1</sup>
$k_3$	2.5	100.00	Yes	Yes	Yes	No <sup>2</sup>
$k_4$	75	4.00	Yes	Yes	Yes	No <sup>2</sup>
$k_5$	5	300.00	Yes	Yes	Yes	No <sup>2</sup>
$k_6$	0.001	100.00	Yes	Yes	Yes	No <sup>1</sup>
$k_7$	3.5	15.00	Yes	Yes	Yes	No <sup>1</sup>
$k_8$	0.00001	2.00	Yes	Yes	Yes	No <sup>2</sup>
$q_R$	0.15	2.33	Yes	No <sup>3</sup>	Yes	No <sup>1</sup>
$\tau$	100	2.00	Yes <sup>4</sup>	Yes	Yes	No <sup>1</sup>

<sup>1</sup> Premature onset of fast phase.

<sup>2</sup> Delayed onset of fast phase.

<sup>3</sup> No discernible dampening of oscillations before onset of fast phase.

<sup>4</sup> Period too long.

dorsal closure (DC) is lost. The choice of these “desirable features” is somewhat subjective, and we have chosen the following four: oscillations sustained for the duration of the Early Phase, dampening of the oscillations during the Slow Phase, an appreciable ratcheting effect in the Slow Phase, and timely onset of the Fast Phase. Tables S2 and S3 report the lower and upper bounds for each of the kinetic parameters, along with information on which of the four features is lost and how. The baseline values were chosen from the literature when available and for those that no sources exist, a value was chosen as to maximize the desirable features stated above. Note that the bounds are reported as multiplicative factors that, when multiplied by the baseline parameter values, yield the thresholds for each parameter.

To illustrate graphically how an essential feature is lost when a certain parameter goes beyond the thresholds in the tables, we plot in Figs. S1 and S2 several solutions over a range of values for  $k_1$  (periphery-to-medial transport rate of aPKC) and  $q_R$

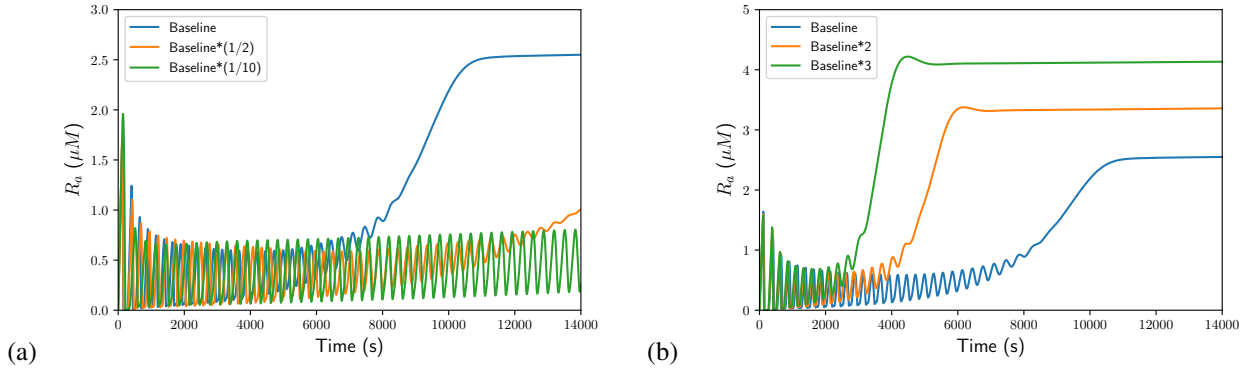


Figure S1: Effect of  $k_1$  on  $R_a$ . (a) Decreasing  $k_1$  causes oscillations to persist for longer, delaying and even losing entirely the ratchet and the transition to the fast phase. (b) Increasing  $k_1$  shortens the early phase and causes premature closure.

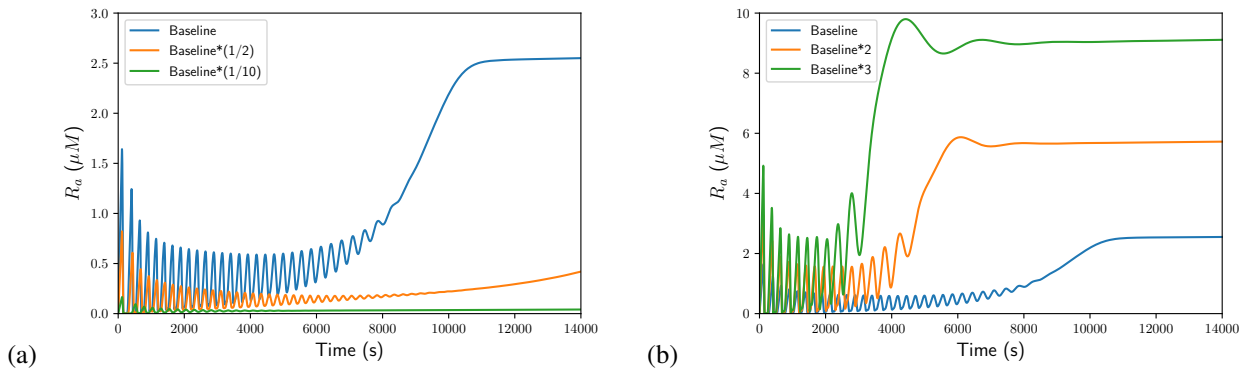


Figure S2: The effect of (a) decreasing  $q_R$  and (b) increasing  $q_R$  on the regulator  $R_a$ .

(source for actomyosin regulator), respectively. Similar sweeps have been carried out for the rest of the parameters and similar trends are seen. As noted in the main text, the qualitative features of DC are most sensitive to the dynamics of the active regulator  $R_a$ . It dictates the dynamics of apicomedial actomyosin and in turn the outcomes in cell oscillation and contraction. Thus, these figures plot  $R_a$  as the dependent variable.

Figure S1(a) shows that decreasing  $k_1$  slows down the entire process. The oscillation of the early phase persists longer. Dampening of oscillation, ratcheting and the onset of the fast phase are delayed or even lost entirely. Consequently, such embryos would fail to close during the normal time frame of DC. Conversely, a large  $k_1$  hastens the advent of ratcheting and the fast phase, at the expense of sustained oscillation of the early phase (Fig. S1b). One would expect premature closure for such embryos. Similar trends are observed for  $q_R$  in Fig. S2. Lower production of the regulator weakens the dynamics, reducing the amplitude of the  $R_a$  and myosin oscillations and eliminating ratcheting and persistent contraction. Such embryos will not contract much nor achieve closure. Elevated  $q_R$ , on the other hand, precipitates the ratcheting and the onset of the fast contraction and shortens the early phase. The dampening of oscillation in the slow phase also becomes indistinct. These embryos will close prematurely.

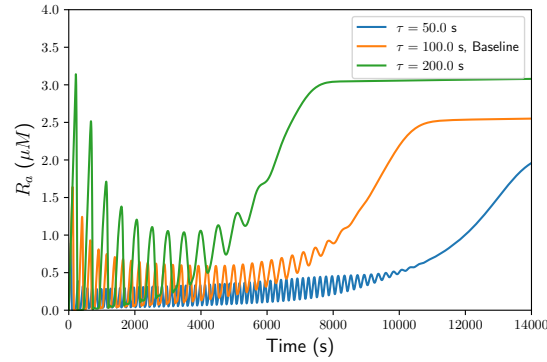


Figure S3: Effect of the delay parameter  $\tau$  on  $R_a$ . A longer  $\tau$  produces a longer period of oscillation.

In fact, similar trends appear through the entire parameter sweep, and we have identified a few general motifs. Across the entire parameter space  $(k_1, \dots, k_8, q_R, \tau)$ , making the reactions slower preserves the oscillatory behavior and in most cases causes them to persist longer. This comes at the expense of the ratchet and onset of the fast phase. Thus, the early phase is prolonged while the slow and fast phases are delayed or even excluded from the duration of the simulation. Contrarily, increasing the kinetic parameters tends to disrupt cell oscillation, shorten or eliminate the early phase, and precipitate the slow and fast phase with a more pronounced ratcheting effect. Premature closure is the typical result.

Among all the parameters, the solution is most sensitive to the Reg production rate  $q_R$ , the aPKC migration rate  $k_1$  and the delay in aPKC migration  $\tau$ . These three exhibit the narrowest and most restrictive ranges for maintaining the four key features. Inspection of Eqs. (1–9) of the main text reveals that  $q_R$  directly affects the  $R_a$  production and appears nowhere else. Thus, its effect on  $R_a$ , which dictates features such as areal oscillation, ratcheting and fast-phase constriction, is unmitigated by other parameters. Similarly,  $k_1$  and  $\tau$  appear only in the transport of aPKC, another key factor in the model. The other kinetic parameters, in contrast, all appear in several equations. Their effects on  $R_a$  or  $A_m$  are modulated by additional parameters and thus less direct and stark. A good example is  $k_3$ . Even though it affects  $R_a$  in Eq. (5),  $k_3$  also affects  $A_m$  and  $AR$ , with  $AR$  further influencing  $A_m$  through the  $k_4$  term of Eq. (3). Consequently, the effect of  $k_3$  on the model outcome is not as acute. Additionally, we found that the main control of the period of oscillation is the delay parameter  $\tau$ . Increasing  $\tau$  lengthens the period, whereas decreasing  $\tau$  elevates the frequency of oscillations (Fig. S3). This result can be rationalized by noting that  $\tau$  is the delay in aPKC transport from the circumference to the medial domain, and the medial aPKC, by recruiting Baz and phosphorylating Reg, is at the root of the actomyosin cycle. Finally, we note that reducing  $k_6$  to 0 has little effect on the model predictions, and in particular maintains the four qualitative features defined in the above. This can be attributed to the already low rate of Baz cluster dissociation in comparison to cluster formation; cluster dissociation is dispensable in the model.

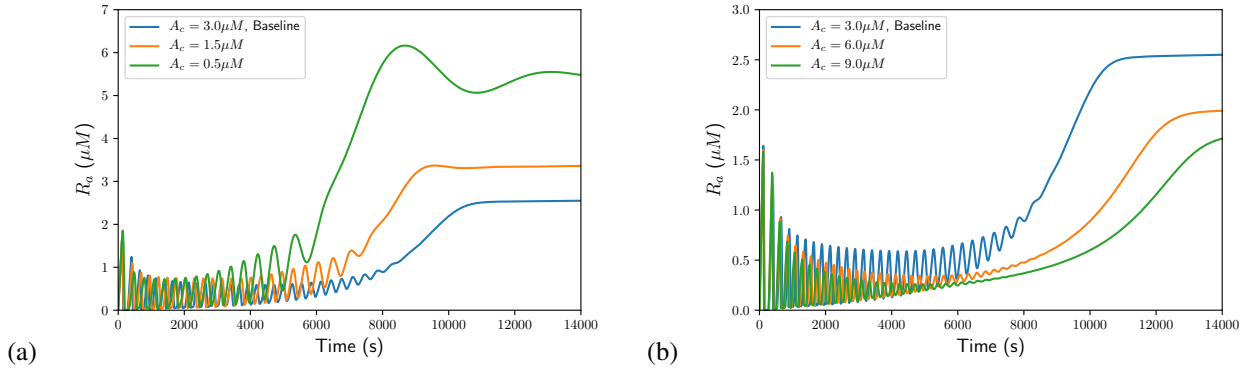


Figure S4: (a) Decreasing the initial circumferential store of aPKC,  $A_c$ , results in aPKC being exhausted prematurely and the embryo would transition into the fast phase too soon. (b) Increasing  $A_c$  results in decreased  $R_a$  concentrations.

### S2.2 Initial conditions

As explained in the main paper, the ratcheting effect and onset of the fast phase are largely the result of depleting the circumferential aPKC store ( $A_c$ ). We have also noted that only a small portion of the initial circumferential Baz ( $B_c$ ) eventually participates in the medial actomyosin cycle. Therefore, we find it necessary to explore the dependence of the active Reg on the initial conditions of the circumferential PAR-proteins. The ranges of  $A_c$  and  $B_c$  that yield desirable behavior are summarized in Table S4.

Table S4: The upper and lower bounds for the initial conditions, given as multiplicative factors.

Parameter	Baseline	Bound	Oscillations	Dampening	Ratchet	Fast Phase
$A_c$ (lower)	3.0	0.25	Yes	No <sup>1</sup>	Yes	Yes
$A_c$ (upper)	3.0	2.00	Yes	Yes	Yes	No <sup>2</sup>
$B_c$ (lower)	3.0	0.50	Yes	Yes	Yes	No <sup>2</sup>
$B_c$ (upper)	3.0	5.00	Yes	Yes	Yes	No <sup>3</sup>

<sup>1</sup> No discernible dampening of oscillations before onset of fast phase.

<sup>2</sup> Delayed onset of fast phase.

<sup>3</sup> Premature onset of fast phase.

Unsurprisingly, we find that  $A_c$  and  $B_c$  have opposite effects on  $R_a$ . Lowering the initial  $A_c$  results in an increase in the overall  $R_a$  (Fig. S4a). Besides, the oscillatory early phase is shortened but has greater amplitude, whereas ratcheting and the slow phase become indistinct and quickly give way to a premature transition to the fast phase. The lower threshold can be put at  $A_c = 0.75 \mu\text{M}$ . Raising the initial  $A_c$ , on the other hand, tends to suppress the level of  $R_a$  (Fig. S4b). This is easily understood from Eqs. (3) and (5) of the main text. The upper bound is around  $A_c = 6 \mu\text{M}$ . Contrarily, decreasing the initial  $B_c$  results in a decrease of  $R_a$  over the course of DC (Fig. S5a). If  $B_c$  is too low, the embryo may stay in a state resembling the early phase for the duration of the entire simulation, with decreased amplitude of the cellular oscillations but very little ratcheting and no transition into the fast phase. At higher  $B_c$ , ratcheting and closure both happen earlier, with stronger actomyosin

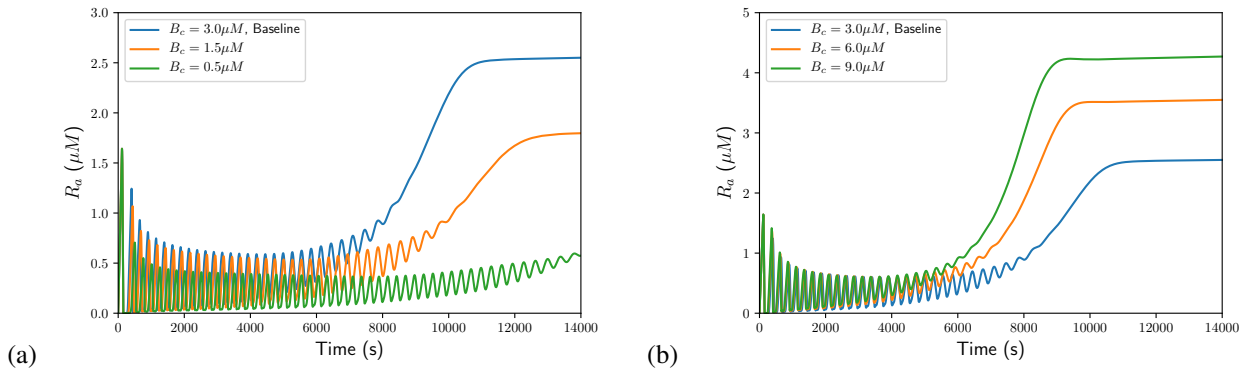


Figure S5: (a) Decreasing the initial circumferential store of Baz,  $B_c$ , results in a longer sustained oscillatory period and delayed onset of the fast phase. (b) Increasing  $B_c$  precipitates ratcheting and the transition to fast phase.

contraction (Fig. S5b). As noted in the main text, however, the model outcome is relatively insensitive to  $B_c$ . The lower and upper thresholds for  $B_c$  are 0.5 and 5 times the baseline value, respectively.

### S3 Cross-correlations

During the early and slow phases, neighboring cells oscillate preferentially in antiphase. This is quantified by computing the cross-correlation of the areal change between neighbors, and averaging over the duration of the early and slow phases and over all 320 pairs of neighbors in the tissue. First, we calculate the instantaneous area  $A_i$  of any given cell  $i$  and its rolling mean over one period ( $T \sim 260$  s):

$$\bar{A}_i(t) = \frac{1}{T} \int_{t-T/2}^{t+T/2} A_i(\tau) d\tau.$$

The difference  $A_i(t) - \bar{A}_i(t)$  indicates the instantaneous state of expansion or contraction of the cell. We then calculate the cross-correlation of  $A_i(t) - \bar{A}_i(t)$  with delay  $\Delta T$  by two different methods. First, we use Python's Numpy.correlate function to calculate the cross-correlation between each pair of neighbors over the duration of the early and slow phase (from  $t = 0$  to 8046 s) and average it over all 320 pairs of neighbors in the AS tissue. We have also calculated the cross-correlation by the following formula (4):

$$F_{cc}(\Delta T) = \frac{\sum_t (A_i(t) - \bar{A}_i)(A_j(t - \Delta T) - \bar{A}_j)}{\sqrt{\sum_t (A_i(t) - \bar{A}_i)^2 \sum_t (A_j(t - \Delta T) - \bar{A}_j)^2}}, \quad (\text{S6})$$

where the summation is over the discrete time steps of our ODE solution within the early and slow phases. We then average  $F_{cc}(\Delta T)$  over all cell-neighbor pairs. Both methods give the same result in Fig. S6(a). The negative peak at  $\Delta T = 0$  demonstrates a preferentially antiphase correlation among neighbors. But the small magnitude (about  $-0.06$ ) reflects the fact that cell neighbors exhibit both antiphase and in-phase correlation during their oscillation (4), and that on average the mechanical coupling has only a weak effect on cell oscillation.

We have also computed the cross-correlation between changes in a cell's area and its medial myosin, relative to their respective rolling mean values over a period  $T$ , averaged over all 121 cells in the AS tissue. Figure S6(b) shows that the area correlates negatively with the myosin, with a delay in time of about 27 s. This is consistent with experimental observations (18), the delay being due to viscous friction on nodal motion. Furthermore, the large magnitude of negative correlation ( $\sim -0.92$ ) indicates that the cell dynamics are primarily dictated by the internal myosin concentration of the cell. In comparison, neighbor-neighbor mechanical coupling plays a minor role in determining cell area oscillation (Fig. S6a).

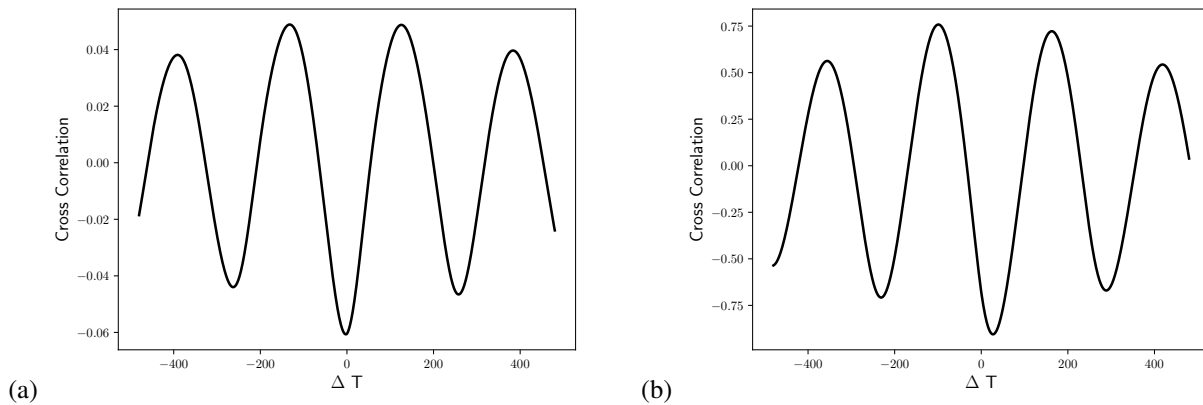


Figure S6: (a) During the oscillation of the early and slow phases, neighboring cells exhibit a preferentially negative cross-correlation in area variation. The negative peak at  $\Delta T = 0$  indicates antiphase oscillation between neighbors. (b) The cell area is strongly anti-correlated with the number of medial myosin motors. The negative peak is offset slightly from  $\Delta T = 0$  because of the viscous friction that hinders nodal motion (Eq. S4).

#### S4 The role of the supracellular actin cable

To explore the significance of the actin cable to dorsal closure and our *ad hoc* treatment in Eq. (S5), we compare the model predictions with and without the actin cable (Fig. S7a). Turning on the actin cable causes a slight decrease in the tissue area subsequently, relative to the case without actin cable, but the effect is minimal (up to 2%). Visually, the actin cable tends to align the outermost cell edges so as to give the tissue a smoother leading edge. This is similar to the prediction of the earlier model of Wang et al. (1). Movie S2 depicts the entire closure process with the actin cable deactivated.

We have conducted further numerical tests on the timing of the actin cable. Figure S7(b) compares three runs with the actin cable activated at different times. An earlier onset does produce a smaller tissue area throughout, but the difference is minuscule. In particular, the instant at which the tissue area peaks before declining, which is taken to be the start of the slow phase, is not affected by the actin cable. Thus, in our model the actin cable is not the trigger for the start of the slow phase.

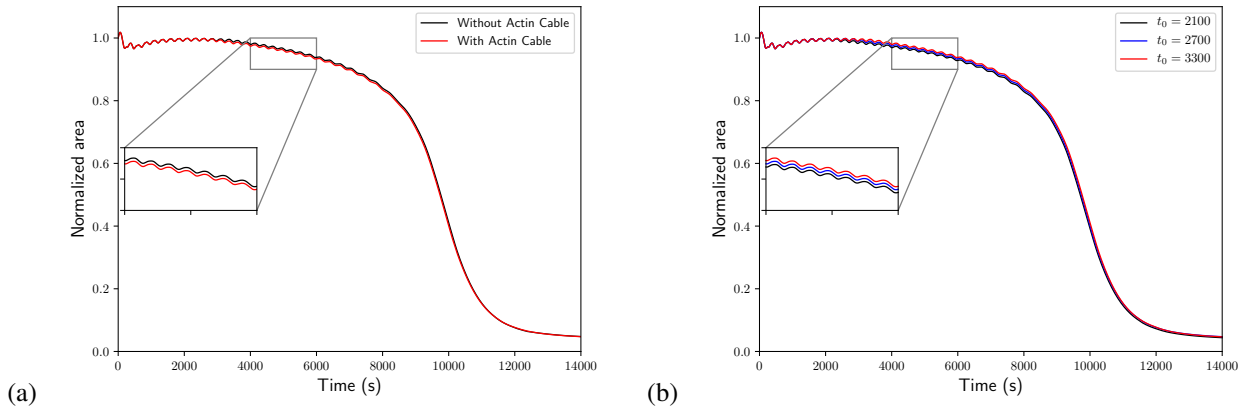


Figure S7: Effect of the actin cable on the temporal evolution of the tissue area. (a) Turning on the actin cable causes a slight decrease in the tissue area, in comparison to the case with no actin cable. (b) Activating the actin cable at different times has a minor effect on dorsal closure; an earlier activation decreases the tissue area slightly.

## S5 Supplementary figures

The following figures are referred to by the main text.

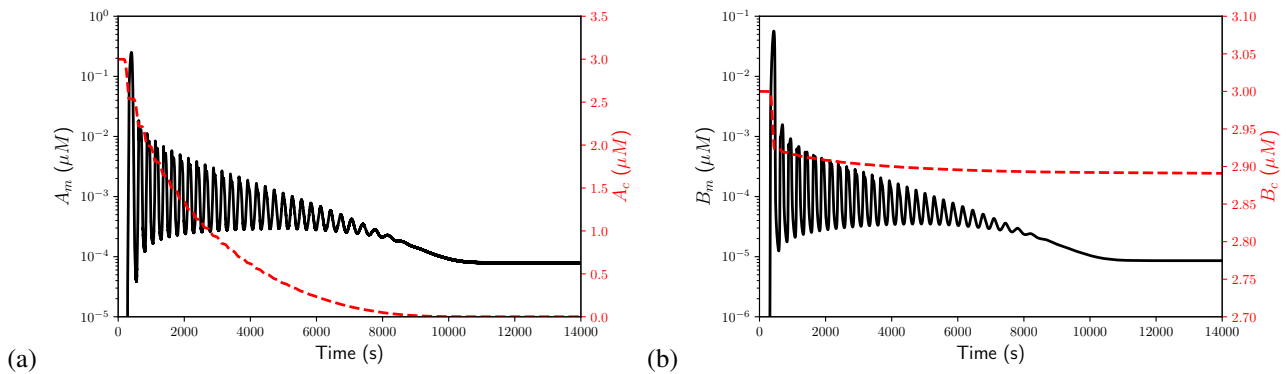


Figure S8: Transport of aPKC and Baz from the circumference to the medial domain. (a) Temporal evolution of  $A_m$  (black solid line) and  $A_c$  (red dashed line). (b) Temporal evolution of  $B_m$  (black solid line) and  $B_c$  (red dashed line).

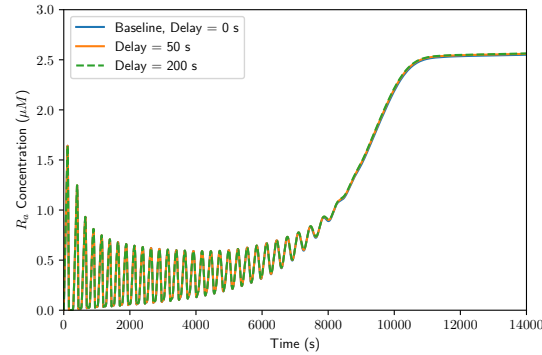


Figure S9: The model does not explicitly account for a time delay in the translocation of Baz from the periphery to the medial domain. Part of the reason is that the high capacity of apicomedial Baz clusters to sequester aPKC implies that only a small fraction of  $B_c$  is transported (see Fig. S8b). The three predictions shown here confirm that adding a Baz transport delay time into the model does not change its prediction significantly.

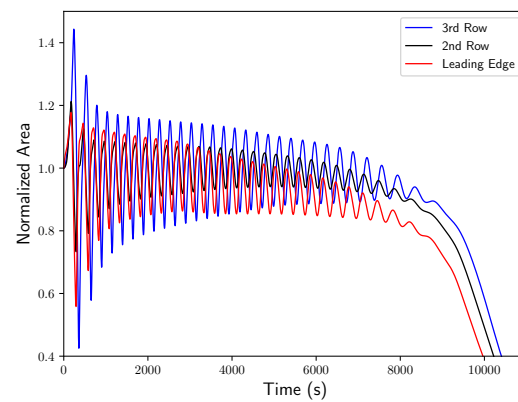


Figure S10: Behavior of a leading edge cell compared with that of cells in the next two rows towards the center. All three cells exhibit the same qualitative dynamics, and the cell oscillations persist for roughly the same length of time. The smaller amplitude of the leading edge cell is due to the blue tension lines representing the epidermis (Fig. 1).

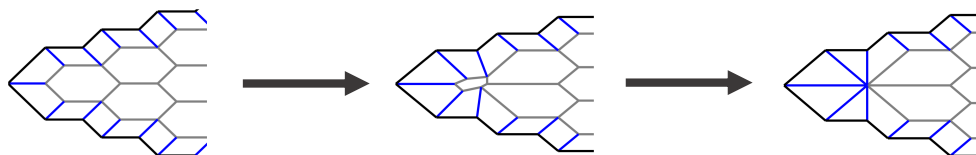


Figure S11: Schematic showing elimination of an “apoptotic” cell from the AS tissue. We model this process by eliminating a cell when its area falls below a threshold of  $1 \mu\text{m}^2$  and all its edges are shorter than  $0.5 \mu\text{m}$ . To maintain the integrity of the model tissue, we collapse the outer nodes of the apoptotic cell onto the central node, a treatment motivated by *in vivo* experiments of Toyama et al. (21) and their Figure 2(a,b). If eliminating a cell brings the opposing epidermis together, as shown here, we consider this the fusion of the epidermis and subsequently fix the location of the central node. This mimics the *in vivo* restructuring process that occurs at the canthi (9). In our model prediction, only two cells are eliminated during the simulation and these are the left- and rightmost cells that form the canthi.

## S6 Supplementary movies

**Movie S1:** Model simulation of the entire dorsal closure process using the baseline parameters of Table S1 of the online Supporting Material. The simulation exhibits the three distinct phases: early (0 – 2352 s), slow (2352 – 8046 s) and fast (8046 – 14000 s). The supracellular actin cable is activated at 2700 s. At the end the amnioserosa has shrunk to about 5% of its initial value.

**Movie S2:** A simulation with the same baseline parameters as Movie S1, but with the supracellular actin cable inactivated. Comparing the two movies, we see that the actin cable has only a cosmetic effect on the dorsal closure process; it smooths the tissue boundary by increasing tension in these edges.

## References

1. Wang, Q., J. J. Feng, and L. M. Pismen, 2012. A cell-level biomechanical model of *Drosophila* dorsal closure. *Biophys. J.* 103:2265–2274.
2. Kovacs, M., K. Thirumurugan, P. J. Knight, and J. R. Sellers, 2007. Load-dependent mechanism of nonmuscle myosin 2. *Proc. Natl. Acad. Sci. U.S.A.* 104:9994–9999.
3. Fernandez-Gonzalez, R., S. de Matos Simões, J.-C. Röper, S. Eaton, and J. A. Zallen, 2009. Myosin II dynamics are regulated by tension in intercalating cells. *Dev. Cell* 17:736–743.
4. Solon, J., A. Kaya-Çopur, J. Colombelli, and D. Brunner, 2009. Pulsed forces timed by a ratchet-like mechanism drive directed tissue movement during dorsal closure. *Cell* 137:1331–1342.
5. Kiehart, D. P., C. G. Galbraith, K. A. Edwards, W. L. Rickoll, and R. A. Montague, 2000. Multiple forces contribute to cell sheet morphogenesis for dorsal closure in *Drosophila*. *J. Cell Biol.* 149:471–490.
6. Hutson, M. S., 2003. Forces for morphogenesis investigated with laser microsurgery and quantitative modeling. *Science* 300:145–149.
7. Gorfinkiel, N., S. Schamberg, and G. B. Blanchard, 2011. Integrative approaches to morphogenesis: Lessons from dorsal closure. *Genesis* 49:522–533.
8. Jayasinghe, A. K., S. M. Crews, D. N. Mashburn, and M. S. Hutson, 2013. Apical oscillations in amnioserosa cells: Basolateral coupling and mechanical autonomy. *Biophys. J.* 105:255–265.
9. Wells, A. R., R. S. Zou, U. S. Tulu, A. C. Sokolow, J. M. Crawford, G. S. Edwards, and D. P. Kiehart, 2014. Complete canthi removal reveals that forces from the amnioserosa alone are sufficient to drive dorsal closure in *Drosophila*. *Mol. Biol. Cell* 25:3552–68.
10. Ducuing, A., and S. Vincent, 2016. The actin cable is dispensable in directing dorsal closure dynamics but neutralizes mechanical stress to prevent scarring in the *Drosophila* embryo. *Nat. Cell Biol.* 18:1149–1160.
11. Pasakarnis, L., E. Frei, E. Caussinus, M. Affolter, and D. Brunner, 2016. Amnioserosa cell constriction but not epidermal actin cable tension autonomously drives dorsal closure. *Nat. Cell Biol.* 18:1161–1172.
12. Saias, L., J. Swoger, A. D'Angelo, P. Hayes, J. Colombelli, J. Sharpe, G. Salbreux, and J. Solon, 2015. Decrease in cell volume generates contractile forces driving dorsal closure. *Dev. Cell* 33:611–621.
13. Hayes, P., and J. Solon, 2017. *Drosophila* dorsal closure: An orchestra of forces to zip shut the embryo. *Mech. Develop.* 144:2–10.

14. Phillips, R., J. Kondev, J. Theriot, and H. Garcia, 2012. *Physical Biology of the Cell*. Garland Science.
15. Forgacs, G., R. A. Foty, Y. Shafirir, and M. S. Steinberg, 1998. Viscoelastic properties of living embryonic tissues: A quantitative study. *Biophys. J.* 74:2227–2234.
16. Besser, A., and U. S. Schwarz, 2007. Coupling biochemistry and mechanics in cell adhesion: A model for inhomogeneous stress fiber contraction. *New J. Phys.* 9:425.
17. Milo, R., and R. Phillips, 2015. *Cell Biology by the Numbers*. Garland Science.
18. Blanchard, G. B., S. Murugesu, R. J. Adams, A. Martinez-Arias, and N. Gorfinkiel, 2010. Cytoskeletal dynamics and supracellular organisation of cell shape fluctuations during dorsal closure. *Development* 137:2743–2752.
19. Gorfinkiel, N., G. B. Blanchard, R. J. Adams, and A. Martinez Arias, 2009. Mechanical control of global cell behaviour during dorsal closure in *Drosophila*. *Development* 136:1889–1898.
20. Machado, P. F., J. Duque, J. Étienne, A. Martinez-Arias, G. B. Blanchard, and N. Gorfinkiel, 2015. Emergent material properties of developing epithelial tissues. *BMC Biol.* 13:98.
21. Toyama, Y., X. G. Peralta, A. R. Wells, D. P. Kiehart, and G. S. Edwards, 2008. Apoptotic force and tissue dynamics during *Drosophila* embryogenesis. *Science* 321:1683–1686.